Piezoelectric Accelerometer with Improved Temperature Stability

by

Wenhao Huang

B.E., University of Pittsburgh, 2019

Submitted to the Graduate Faculty of the

Swanson School of Engineering in partial fulfillment

of the requirements for the degree of

Master of Science in Mechanical Engineering

University of Pittsburgh

2021

UNIVERSITY OF PITTSBURGH

SWANSON SCHOOL OF ENGINEERING

This thesis was presented

by

Wenhao Huang

It was defended on

April 8, 2021

and approved by

Qing-Ming Wang, Ph.D., Professor
Department of Mechanical Engineering and Materials Science

Patrick Smolinski, Ph.D., Assosiate Professor
Department of Mechanical Engineering and Materials Science

Heng Ban, Ph.D., Professor
Department of Mechanical Engineering and Materials Science

Thesis Advisor: Qing-Ming Wang, Ph.D., Professor
Department of Mechanical Engineering and Materials Science

Piezoelectric Accelerometer with Improved Temperature Stability

Wenhao Huang, M.S.

University of Pittsburgh, 2021

Piezoceramic materials like PZT allow the manufacturing of piezoelectric sensors with advantages including high sensitivity, low price, and easy to shape. However, it is also featured with the pyroelectric effect, which brings extra charge generation with temperature variations. Those charges caused by the thermal effect contribute to errors in the sensor measurement result. Theoretically, the appropriate configuration of the sensor would neutralize the thermal effect. In this thesis, a triple layer piezoelectric sensor with a parallel connection would be used to check its thermal stability at elevated temperatures. The thesis begins with reviewing the fundamental concepts of piezoelectricity. The following section contains the analysis of the relationship between the different external inputs and the output of a triple layer sensor. The experiment is designed to put the triple layer sensor in a chamber with a temperature control system to test its performance at around 35 ℃ with sinusoidal excitation input. A unimorph sensor would be set as the reference group so that the result of the triple layer sensor could have a comparison with. The cancellation of the temperature effect in the triple layer sensor successfully reduces the output deviation to an acceptable level. Meanwhile, the unimorph structure sensor exhibits obvious instability under the same conditions.

Table of Contents

List of Tables

List of Figures

Preface

First and foremost, I would like to express my sincere gratitude to my thesis advisor, Dr. Qing-Ming Wang, for his guidance and support throughout the process. With his help, I have learned a lot during my master thesis.

I also want to appreciate my colleague, Gongyuan Liu, Zihao Zhong, Ruixin Feng, and Weibo Gao, and Wenxiang Qiang in the laboratory. Particularly, I want to share my thanks to the discussion and cooperation with Gongyuan Liu on our work.

To my friends, Meixian Jiang, I want to deliver my thanks for your encouragement and for sharing your happiness with me in the hard pandemic period. Also, I would like to thank my roommate Zhefan Xu, who makes my life in the United States not alone.

Finally, I want to express my profound feeling of gratitude to my family, who support me to finish my study in a foreign land and will always love me.

1.0 Introduction

The application of a piezoelectric sensor to test static and dynamic load such as pressure or vibration is well established in many areas such as automotive, aerospace, and other daily control systems. High sensitivity, no extra energy input required, simple structure, and low production cost make it a popular commercial choice. However, the stability of the sensor is dependent on many factors. A crucial aspect of the working environment is the temperature that should be considered for many areas. One typical example is the engine, where the thermal cycle brings heat that makes temperature rising. The sensors to detect the status of the engine are usually placed inside next to the component needed to be checked, which means it must work properly under high temperatures. [1]

1.1 Background of Piezoelectricity

The sensor usually contains piezoelectric materials to transfer mechanical energy into electric form by the piezoelectric effect. The word piezoelectric effect, which the prefix Piezo comes from the Greek word push, describes the phenomenon of electric charge accumulating due to mechanical pressure applied on the materials. This effect was first discovered in 1880 by Pierre and Jacques Curie. In the next year, they found the phenomenon that applying a voltage across this kind of material, a mechanical deformation would be observed. More specifically, the mechanical energy transaction to electrical energy is called the direct piezoelectric effect, and from electrical to mechanical is called the reverse piezoelectric effect.

The following diagram includes Quartz crystal (SiO_2) helps to understand the piezoelectric effect better (Figure 1.1).

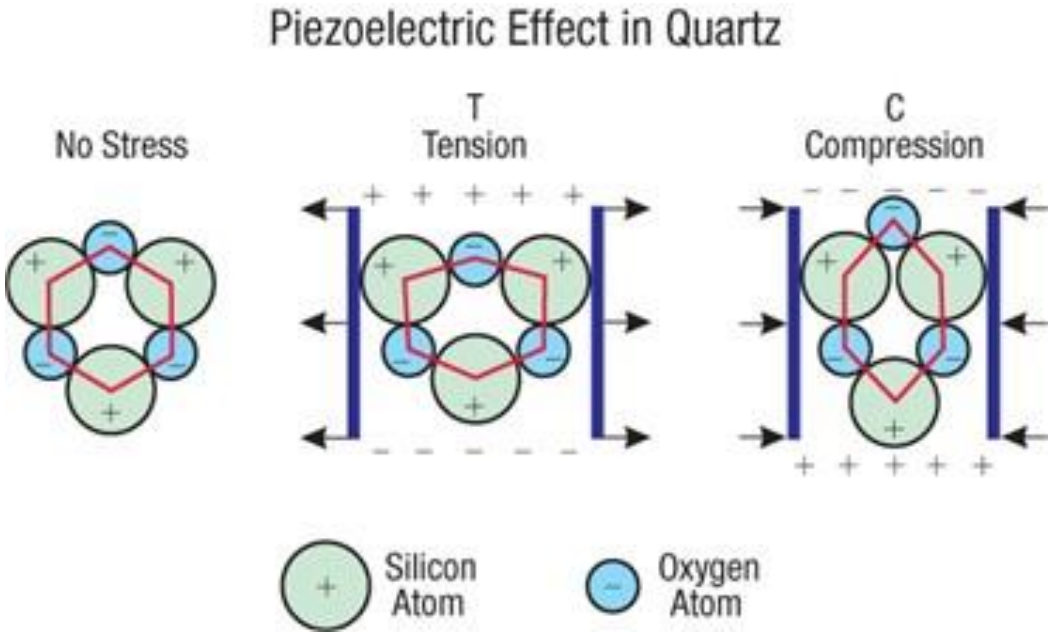

Figure 1.1.1 Quartz Crystal at rest and under different external load [2]

Starting with no external force, connecting the center of all atoms and the lines form a regular hexagon. The geometry property of the structure indicates all three dipoles are evenly distributed. Therefore, the centers of positive and negative charges overlap, and no electric dipole moment exists. The molecule is in a balanced state. Once an external force is applied, the charge center would be slightly away from the original position, and a dipole moment would appear inside the material. The magnitude of the moment depends on the distance between the center of negative and positive charges. Then, the charges would be induced on the surface of the material to resist the dipole moment change. Tension and compression would cause an opposite result of charge accumulating since they move the charge centers in opposite directions.

An extended period after discovering the piezoelectric effect, only natural crystal with the weak piezoelectric effect was available for scientists to develop piezoelectricity-based tools as the

material. Although sonar was invented based on the natural crystal to detect the submarine in 1917, and it was the first successful application outside the laboratory. A large scale of applications did not come true until World War 2, when new kinds of materials were discovered. Encouraged by the success of sonar and the potential of the piezoelectric effect, groups of scientists discovered a new kind of synthetic material named ferroelectrics which was much more sensitive than natural crystal [3]. The first human-made material contains piezoelectricity was mixed oxide compound barium titanite ($BaTiO_3$). The advantages included not only high sensitivity but also easy to manufacture and relatively low cost to produce. Then, it is the lead zirconate titanate (PZT), a new following material is found to be piezoelectric and became the most widely used one until nowadays. A higher working temperature and better sensitivity are performed on PZT materials compared to $BaTiO_3$ [4]. Those materials extended the border of the piezoelectric effect applications and still could be seen in modern industrial equipment.

Ceramic materials, like PZT, $BaTiO_3$, all consist of the unit cell in perovskite structure (Figure 1.2) that makes the charge generation principle slightly different from the Quartz crystal. Typically, the O^{2-} ions occupy the center of the surface, and other positive ions are placed at the corner or the center of the structure. One important feature of those materials is that above the Curie temperature, which varies with the different materials, the structure is symmetrical. No dipole moment exists inside the cells, as shown in Figure 1.2 (a). While below the Curie temperature, the structure is no longer in symmetry and electric dipole arises with the displacement of the atoms (Figure 1.2(b)).

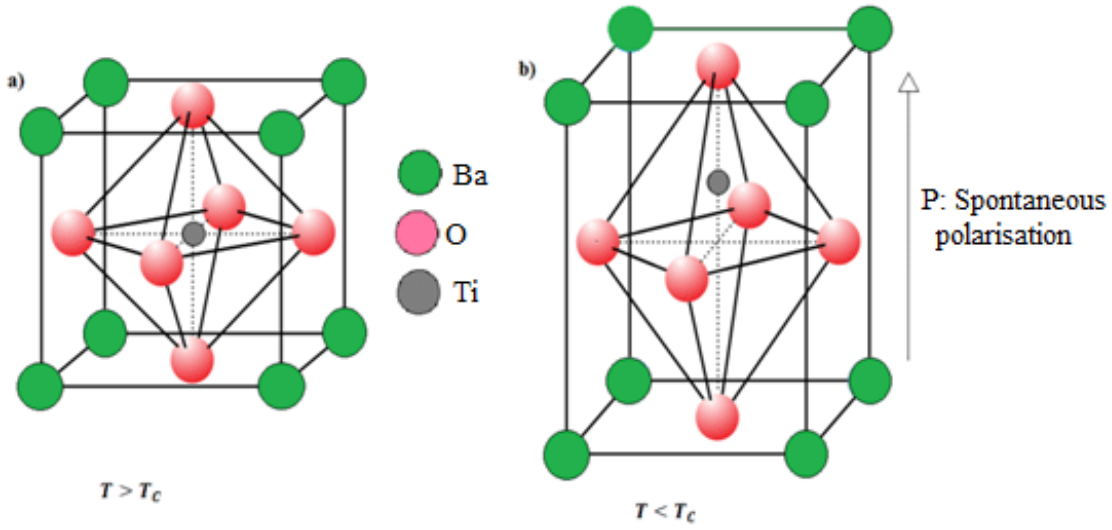

Figure 1.1.2 Crystal structure (a) above the Curie Temperature (b) below the Curie Temperature [5]

The region that contains adjoining dipoles is called the domain, and each domain has its direction. The materials themselves exhibit no polarization with the randomly aligned domains (Figure 1.3 (a)). It is because the polarization of domains would be neutralized with each other.

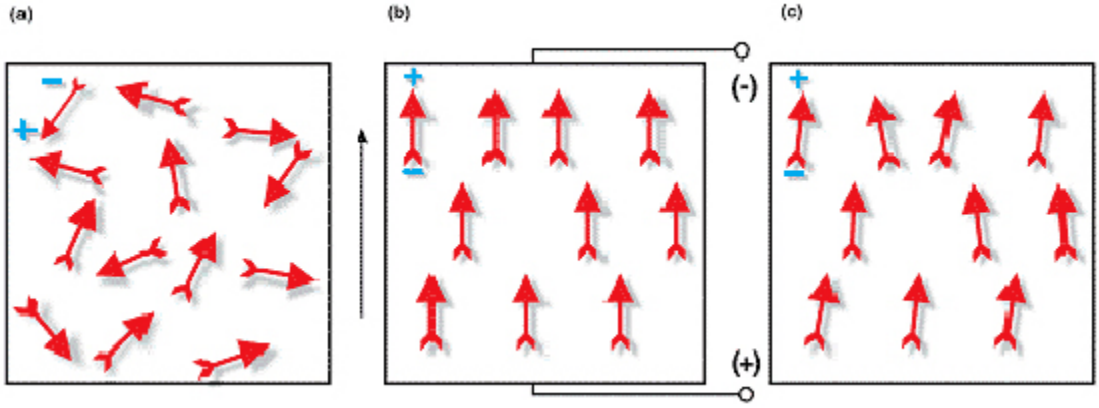

Figure 1.1.3 (a) The distribution of the domains before polarization (b)The distribution under electric field (c) The remnant polarization [6]

Based on that, the external force would not be able to trigger a charge generation. To have a desired polarized material, one available method is to put the material under a high direct current electric field while the temperature below the Curie temperature. The electric field forces all domains to point in the same direction as the electric field (Figure-1.3(b)). After the field is removed, the alignment would not return to the original state and causes a remanent polarization in the material (Figure-1.3(c)).

Applying a large reverse electric field also could reverse the direction of the polarization. That phenomenon introduces the concept of the hysteresis loop. The loop connects the electric field *E* to polarization *P* with an interchangeable relation, which the relationship is illustrated in Figure 1.4.

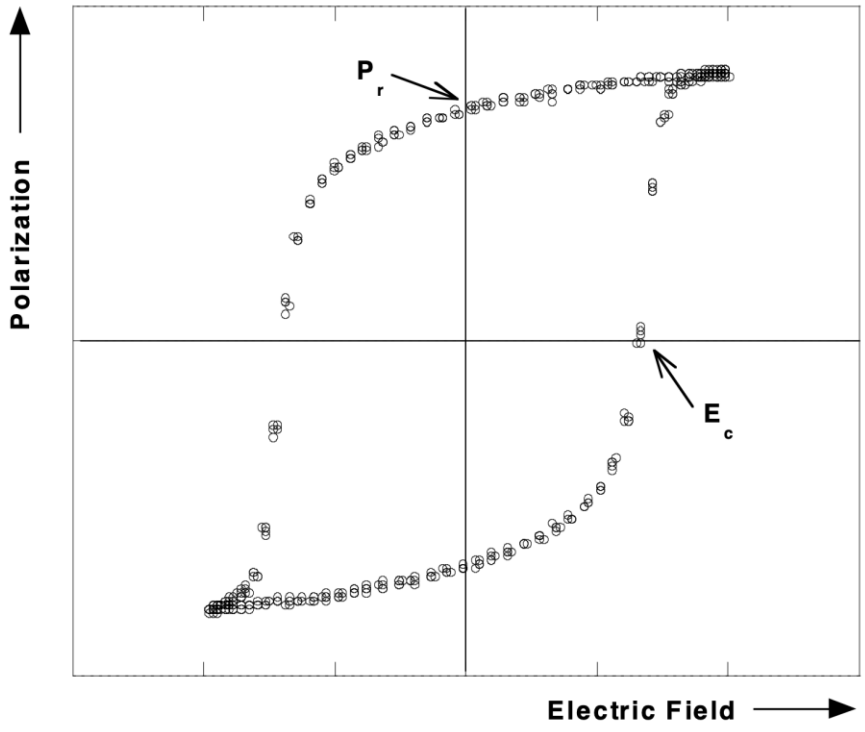

Figure 1.1.4 Hysteresis loop of a piezoelectric ceramic [7]

The two most important characteristics are coercive electric field E_c and remnant polarization P_r. The definition of E_c is the electric field when the polarization is zero and P_r is the polarization when the electric field is zero. The loop is said to be saturated once these two variables no longer changed and can be determined.

1.2 PZT Material Constitutive Equation

The three-dimensional linear piezoelectric constitutive equation for piezoelectric materials is introduced to describe the electromechanical properties of materials. There are four field variables if neglecting the temperature effect, stress components (T_{ij}), strain components (S_{ij}), electric field components (E_k), and the electric displacement components (D_k). For the coordinates system, the positive direction of the polarization is the z-axis representing by 3, x and y occupy 1 and 2. The numbers 4,5,6 represent the shear on x-, y-, z-axis.

Since four field variables are involved, the standard form of the piezoelectric constitutive questions can be given in four different forms by choosing two variables to conduct the other two variables. The equation sets start with d-form:

$$D_m = \varepsilon^T{}_{mn} E_n + d_{mkl} T_{kl} \tag{1.1}$$

$$S_{ij} = d_{ijn} E_n + s^E{}_{ijkl} T_{kl} \tag{1.2}$$

e-form:

$$D_m = \varepsilon^S{}_{mn} E_n + e_{mkl} S_{kl} \tag{1.3}$$

$$T_{ij} = -e_{ijn} E_n + c^E{}_{ijkl} S_{kl} \tag{1.4}$$

g-form:

$$E_m = \beta^T{}_{mn} D_n - g_{mkl} T_{kl} \tag{1.5}$$

$$S_{ij} = g_{ijn} D_n + s^D{}_{ijkl} T_{kl} \tag{1.6}$$

h-form:

$$E_m = \beta^S{}_{mn} D_n - h_{mkl} S_{kl} \tag{1.7}$$

$$T_{ij} = -h_{ijn} E_n + c^D{}_{ijkl} S_{kl} \tag{1.8}$$

where ε is the electric permittivity, s is the elastic compliance constants, d is the piezoelectric strain constant, c is the elastic stiffness constant, e is the piezoelectric stress constant, g is the piezoelectric voltage constant, h is the piezoelectric charge constant, and β is the impermeability.

The form best describes the behavior of piezoelectric sensor is d-form which picks mechanical stress and electric field as independent variables. The matrix form of the equation (1.1) and (1.2) is:

$$\begin{bmatrix} D_1 \\ D_2 \\ D_3 \end{bmatrix} = \begin{bmatrix} \varepsilon_{11}^T & \varepsilon_{12}^T & \varepsilon_{13}^T \\ \varepsilon_{21}^T & \varepsilon_{22}^T & \varepsilon_{23}^T \\ \varepsilon_{31}^T & \varepsilon_{32}^T & \varepsilon_{33}^T \end{bmatrix} \begin{bmatrix} E_1 \\ E_2 \\ E_3 \end{bmatrix} + \begin{bmatrix} d_{11} & d_{12} & d_{13} & d_{14} & d_{15} & d_{16} \\ d_{21} & d_{22} & d_{23} & d_{24} & d_{25} & d_{26} \\ d_{31} & d_{32} & d_{33} & d_{34} & d_{35} & d_{36} \end{bmatrix} \begin{bmatrix} T_1 \\ T_2 \\ T_3 \\ T_4 \\ T_5 \\ T_6 \end{bmatrix} \tag{1.9}$$

$$\begin{bmatrix} S_1 \\ S_2 \\ S_3 \\ S_4 \\ S_5 \\ S_6 \end{bmatrix} = \begin{bmatrix} d_{11} & d_{21} & d_{31} \\ d_{12} & d_{22} & d_{32} \\ d_{13} & d_{23} & d_{33} \\ d_{14} & d_{24} & d_{34} \\ d_{15} & d_{25} & d_{35} \\ d_{16} & d_{26} & d_{36} \end{bmatrix} \begin{bmatrix} E_1 \\ E_2 \\ E_3 \end{bmatrix} + \begin{bmatrix} s_{11}^E & s_{12}^E & s_{13}^E & s_{14}^E & s_{15}^E & s_{16}^E \\ s_{21}^E & s_{22}^E & s_{23}^E & s_{24}^E & s_{25}^E & s_{26}^E \\ s_{31}^E & s_{32}^E & s_{33}^E & s_{34}^E & s_{35}^E & s_{36}^E \\ s_{41}^E & s_{42}^E & s_{43}^E & s_{44}^E & s_{45}^E & s_{46}^E \\ s_{51}^E & s_{52}^E & s_{53}^E & s_{54}^E & s_{55}^E & s_{56}^E \\ s_{61}^E & s_{62}^E & s_{63}^E & s_{64}^E & s_{65}^E & s_{66}^E \end{bmatrix} \begin{bmatrix} T_1 \\ T_2 \\ T_3 \\ T_4 \\ T_5 \\ T_6 \end{bmatrix} \tag{1.10}$$

There exist further symmetries within piezoelectric materials. Therefore, remarkable reduction of independent components could be given. The matrix d-form constitutive equation for the material of crystal class 4mm (PZT and $BaTiO_3$) and 6mm could be simplified to [8]:

$$\begin{bmatrix} D_1 \\ D_2 \\ D_3 \end{bmatrix} = \begin{bmatrix} \varepsilon_{11}^T & 0 & 0 \\ 0 & \varepsilon_{11}^T & 0 \\ 0 & 0 & \varepsilon_{33}^T \end{bmatrix} \begin{bmatrix} E_1 \\ E_2 \\ E_3 \end{bmatrix} + \begin{bmatrix} 0 & 0 & 0 & 0 & d_{15} & 0 \\ 0 & 0 & 0 & d_{15} & 0 & 0 \\ d_{31} & d_{31} & d_{33} & 0 & 0 & 0 \end{bmatrix} \begin{bmatrix} T_1 \\ T_2 \\ T_3 \\ T_4 \\ T_5 \\ T_6 \end{bmatrix} \tag{1.11}$$

$$\begin{bmatrix} S_1 \\ S_2 \\ S_3 \\ S_4 \\ S_5 \\ S_6 \end{bmatrix} = \begin{bmatrix} 0 & 0 & d_{31} \\ 0 & 0 & d_{31} \\ 0 & 0 & d_{33} \\ 0 & d_{15} & 0 \\ d_{15} & 0 & 0 \\ 0 & 0 & 0 \end{bmatrix} \begin{bmatrix} E_1 \\ E_2 \\ E_3 \end{bmatrix} + \begin{bmatrix} s_{11}^E & s_{12}^E & s_{13}^E & 0 & 0 & 0 \\ s_{12}^E & s_{11}^E & s_{13}^E & 0 & 0 & 0 \\ s_{13}^E & s_{13}^E & s_{33}^E & 0 & 0 & 0 \\ 0 & 0 & 0 & s_{44}^E & 0 & 0 \\ 0 & 0 & 0 & 0 & s_{44}^E & 0 \\ 0 & 0 & 0 & 0 & 0 & 2\left(s_{11}^E - s_{12}^E\right) \end{bmatrix} \begin{bmatrix} T_1 \\ T_2 \\ T_3 \\ T_4 \\ T_5 \\ T_6 \end{bmatrix} \tag{1.12}$$

The pressure sensor is designed based on the direct piezoelectric effect that transforms the mechanical energy into electrical energy, so equation (1.11) is the one interested at. The relation between mechanical stress and charge generation is desired for sensor application. In this situation, the sensor is usually working without applied voltage. Therefore, the electric field *E* is zero. The equation becomes a more particular form:

$$\begin{bmatrix} D_1 \\ D_2 \\ D_3 \end{bmatrix} = \begin{bmatrix} 0 & 0 & 0 & 0 & d_{15} & 0 \\ 0 & 0 & 0 & d_{15} & 0 & 0 \\ d_{31} & d_{31} & d_{33} & 0 & 0 & 0 \end{bmatrix} \begin{bmatrix} T_1 \\ T_2 \\ T_3 \\ T_4 \\ T_5 \\ T_6 \end{bmatrix} \tag{1.13}$$

Equation (1.13) illustrates three piezoelectric constants with different directions involved in the transformation from mechanical to electrical energy. Three different types of sensors are named by the constants d_{31}, d_{33}, and d_{15}. The first subscript implies the direction normal to the surfaces that charges would be accumulated on, and the second one is the direction of the stress applied to generate the charges. Taking d_{33} for example, the stress is along the 3-direction, and the electrodes are on the surfaces formed by 1-2 axis where direction-3 is normal to it, as Figure 1-5 shown. Following the rule, d_{31} mode means the stress is along the direction-1 and the surface of the electrodes to collect charges is the same as d_{33}. As for d_{15}, that means the stress is the shear on direction-2 while the electrode is on the surface formed by direction-2 and 3. However, since it is working based on shear stress, it is not such common as d_{31} and d_{33} mode sensor.

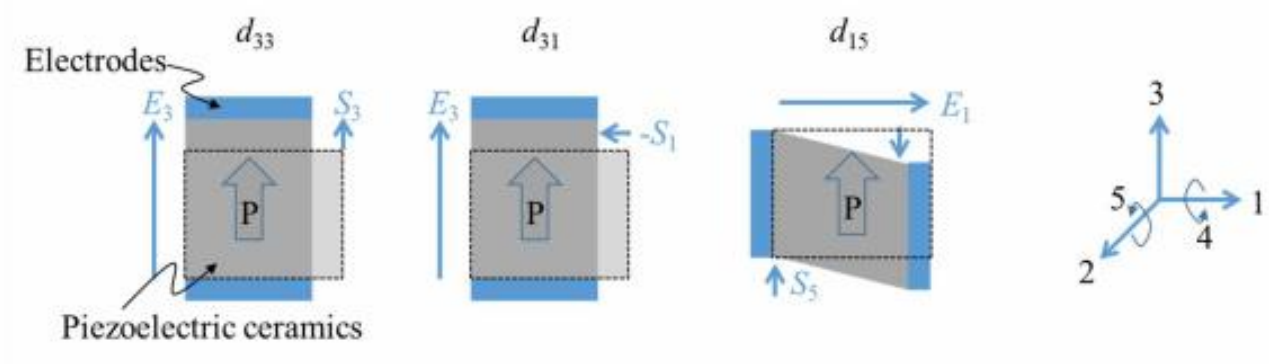

Figure 1.1.5 Mode of operation for piezoelectric sensor [9]

The voltage between the electrode is given by:

$$V = \frac{Q}{C_p} \tag{1.14}$$

where C_p is the capacitance of the piezoelectric sensor. For parallel arrangement with two same plates, the capacitance could be determined by:

$$C_p = \varepsilon_0 \frac{A}{t} = \frac{Lw\varepsilon_0}{t} \tag{1.15}$$

where L is the length of the PZT material, t is the thickness, and w is the width. Substitution equation (1.15) to equation (1.14) and using the constant of d_{31} mode sensor, it becomes:

$$V_{31} = \frac{DA}{C} = \frac{d_{31}}{\varepsilon_{11} L} F_1 \tag{1.16}$$

For d_{33} mode:

$$V_{33} = \frac{d_{33} t}{\varepsilon_{33} lw} F_3 \tag{1.17}$$

In equations (1.16) and (1.17), all variables except force applied F are related to the property of the PZT materials, which means they will not vary with the change of the external force. It indicates the voltage generated would have a linear relationship with F.

1.3 Temperature Effect of PZT Materials

Ferroelectric materials are usually both piezoelectric and pyroelectric. It means that the materials would respond to temperature change similarly as the force due to the pyroelectric effect. A short formula could evaluate this charge generation under temperature change [10]:

$$\frac{dQ}{dt} = k \frac{dT}{dt} \tag{1.18}$$

where Q is the charge generated by the temperature effect, T is the temperature, t is the time, and k is a proportional constant. Once the environment temperature increases or decreases, the charge movement inside the materials would no longer only be influenced by the mechanical pressure. It is also impossible to tell the charges generated by those two effects apart, and it would significantly

reduce the accuracy of the measurement results. Moreover, elevated temperature reduces the polarization of material, and causes reduced output voltage.

A bimorph structure sensor with two sheets of piezoelectric materials that are bonded together can theoretically achieve mutual cancellation of the temperature-generated charges by a specific configuration. One alternative method for extreme temperature conditions (>900 ℃) is choosing other materials rather than PZT. Except for the change of the electromechanical properties, the material phase change and increased attenuation of acoustic waves from mechanical loss must also be considered. [11]

1.4 Typical Structure of The Sensor

Three different mechanical structures are used in the design of the sensors: axial compression, flexural, and shear mode. They can test force, pressure, and vibration by appropriately related the input load with the output voltage by some modifications to the design.

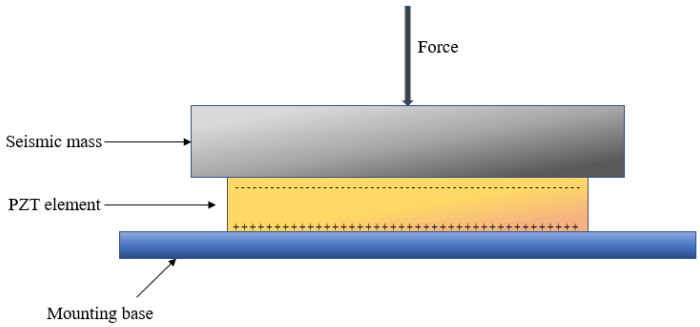

Figure 1.1.6 Compression force sensor

The compression sensor is working based on the d_{33} mode introduced in the previous section. The pressure is applied along the center axis of the material, which is parallel to the direction of polarization, resulting in a voltage in the same direction of the force. A simple structure sensor could be assembled based on that idea. The structure is shown in Figure 1.6.

Different kinds of load could be applied to the seismic mass and transduce to the PZT element to generate voltages. Stable and straightforward configuration brings high sensitivity output, whereas it also brings a high temperature transient sensitivity and base strain sensitivity. The shortcoming of the compression sensor is that it could not have an accurate result in the critical working environment.

The flexural sensor designed in d_{31} mode is shown in Figure 1.7. Taking the force sensor as an example. The force is applied on the transverse axis to extend the PZT element horizontally, and the voltage is still appearing along the vertical direction z.

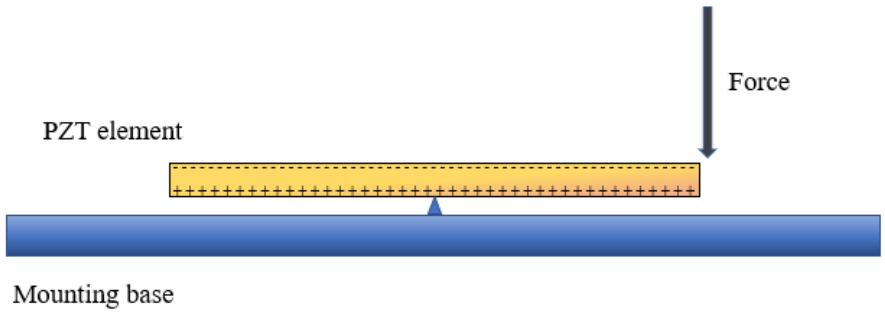

Figure 1.1.7 Flexularl type Sensor

Mentioned in the former section, the temperature effect could be reduced to an acceptable level by self-cancellation of d_{31} mode sensor consists of two same PZT elements. However, the

complex structure arises a frequency limitation. Extreme high or low frequency both make the result inaccurate. The useable region of the frequency would be discussed in the further section.

As for the shear mode sensor shown in Figure 1.8, the piezoelectric element is installed on the side of the center post with a seismic mass on the top of the piezoelectric element. This structure is generally used in accelerometers. The advantage of the shear mode includes the relatively wide frequency range, low sensitivity to directional selection or temperature fluctuation. It could be capable for the different environments with the high cost and complex structure.

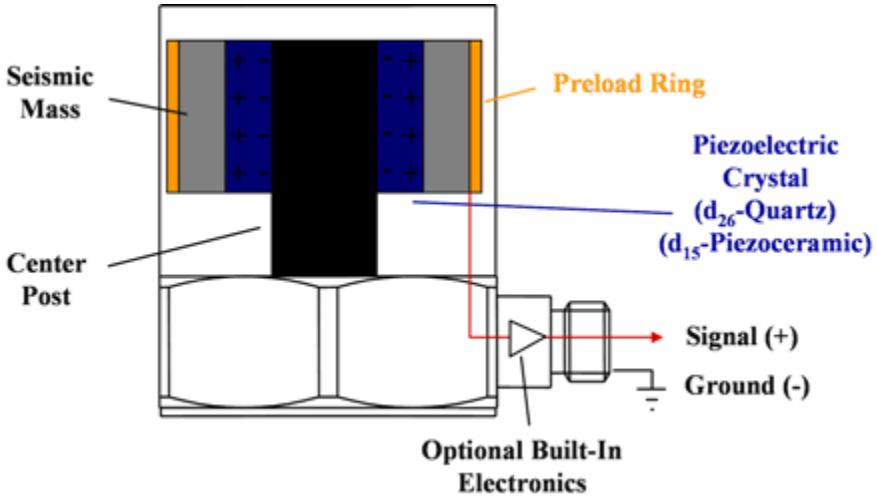

Figure 1.1.8 Schematic of shear piezoelectric accelerometer [12]

1.5 Advantage and Disadvantage of Piezoelectric Sensor

After several decades of development since the discovery, sensors made of piezoelectric materials have occupied a large market of the products ranging from our daily tools to some advancing applications such as Structural Health Monitoring [13]. Nowadays, even the reliability and stability of the piezoelectric sensor have been proved, scientists still intend to optimize the performance of the current design.

Piezoelectric sensor taking advantage of its material properties compared with the traditional mechanical sensor. For example, it is convenient to fabricate and shape a piezoelectric ceramic at a low cost. Ceramic itself is also featured with a large modulus of elastic around $10^{10}\mathrm{N/m^2}$ which means only a little strain would generate a considerable output. However, ceramic is also stiff and brittle. It is hard to be fitted on a curved surface since the bending angle of the ceramic is limited. The substituting method is to use the piezoelectric polymer as the material, which is expensive to fabricated [13].

The most obvious disadvantage for the piezoelectric pressure sensor is that it could not measure the static pressure but only the dynamic pressure. The charge is generated by the defection of the material. Once the pressure is static, the number of charges accumulated on the electrodes fixed. The sensor contains self-capacitance and self-resistance. Therefore, the signal would decay slowly due to the loss of electrons. As a result, there is no voltage difference existing. One more disadvantage is the temperature effect mentioned before. Most of the piezoelectric sensor is sensitive to the temperature change, which produces extra charges and leads to an error in the final output.

As a result, the piezoelectric pressure sensor should be deployed to measure the dynamic pressure and avoid a high-temperature environment unless it is specially designed for this condition to have the best performance.

2.0 Fabrication and Theoretical Analysis of PZT Piezoelectric Sensor

The development and some fundamental concepts of the piezoelectric sensor and its properties are introduced in the previous section. Furthermore, the objective of this research is to design and build a piezoelectric PZT accelerometer that could endure a small range of temperature frustration. As mentioned before, PZT material is selected due to its fast response, low cost, and tiny size. However, PZT material is also sensitive to temperature change. The thermal effect triggers charge generation that is not desired in the measurement. This chapter would focus on the process of establishing a sensor to test vibration, including the material manufacturing steps and sensor structure design and analysis.

2.1 Fabrication and Polarization of The PZT Element

The advantage of PZT material has been mentioned many times before, including the higher sensitivity compared to natural crystal, easy to manufacture and shape in a low cost as well as its excellent stiffness. It is also known that the PZT material is brittle, which means it could not withstand a large bending moment. To avoid this weak point, a new PZT film fabricating process named tape-casting developed by Lifeng Qin brings the possibility to produce a more flexible piezoelectric PZT sensor since it could control the dimension of the PZT element in the unit of micrometer [14].

The first step of the process is to prepare the powders with a Zr:Ti ratio at 52:28 with additional niobium oxide and lanthanum oxide. To get the PZT powders with an average particle

diameter in the sub-micrometer range, the material includes PbO, ZrO_2, and TiO_2 with additives were mixed by the ball billing. After drying, calcination, and fine vibration grinding, these mixed powders, an organic binder and other organic additives are put together to form the slip for tape-casting. The aqueous and nonaqueous solvents are both used for binders. A slurry consists of PZT powder (75to 86 wt%) with a dispersant (1 to 2 wt%) and deionized water (13 to 124 wt%) is used for the aqueous binder system. After finishing the grinding process, the slurry is mixed with a dispersant (33% TRITON-100 solution in deionized water) and a wetting agent (33% TRION CF-10) to create the slip for tape-casting. Refer to non-aqueous binder system, 54 wt% solvent, binder polymer solution (43wt% acrylic resin), and 3 wt% plasticizer with PZT power was mixed to be used as the slip for tape-casting.

The following step is de-airing and casting. The customized belt-casting system shown in Figure 2.1 allows casting the PZT sheet with different thicknesses.

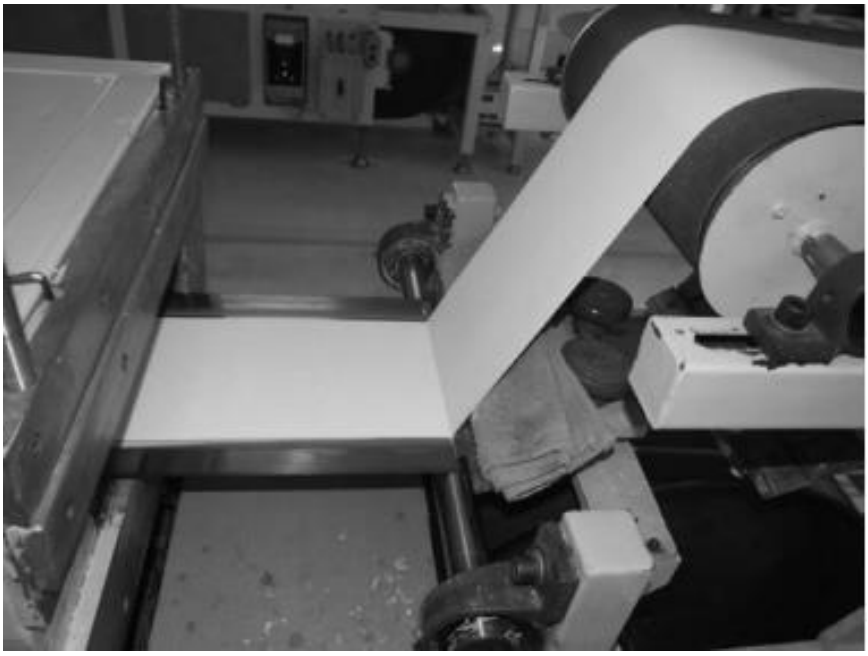

Figure 2.1 The PZT sheet casting machine [14]

Then the sheet is shaped into the desired geometry to be binder burnout and sintering at a high temperature. The next step is coating the sliver electrode on both sides of the PZT element. The final product is shown in Figure 2.2.

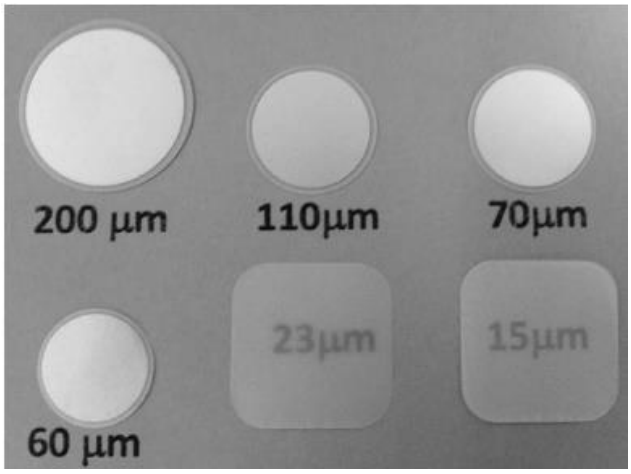

Figure 2.2 PZT films with different dimensions [14]

One more step is required before the PZT film to be placed in the sensor. The polarization of the material is achieved by putting it in the silicone oil at a temperature of 105℃ and connected the electrode with a high DC voltage to apply an electric field along the z-direction for an hour and a half.

Figure 2.3 General d_{33} meter

The value of the d_{33} constant could be measured by the d_{33} meter shown in Figure 2.3. The sign of the constant measured by the meter could also indicate the direction of the polarization where the positive sign means the polarization direction is in the negative z-direction and the negative sign means polarization is in the positive z-direction. The d_{33} constant for the PZT element in this thesis is around 200.

2.2 Design of The Sensor

The first step of the design is to determine the mode of the sensor used. d_{33} mode sensor is simple in structure and easy to assemble and install, but the stress and strain are along the same axis as the external force, which makes it less sensitive than d_{31} mode senor with the same thickness. It is because in d_{31} mode, the force is at the transverse axis, which stretches the element in x or y direction, so the radial stress and transverse strain are much larger than the normal stress and strain in d_{33} mode. In addition, the simple structure consists of only one PZT ceramic makes it hard to resist the thermal effect by any method. As a result, d_{31} mode sensor is taken into consideration for this thesis. The d_{31} mode sensor could be built based on several configurations such as unimorph and bimorph. The choice of configuration would be discussed below.

Another thing that needs to evaluate is the working frequency of the d_{31} mode sensor. Functioning as an accelerometer, the usable frequency of the sensor is an aspect to concern about. The range of the frequency should be as extensive as possible to fit the complicated working environment.

2.2.1 Unimorph Structure Sensor

The arrangement of the unimorph structure is shown in Figure 2.4. The prefix uni implies only one PZT element is covered on a substrate by Epoxy biner. The dimension of the substrate should be slightly larger than The PZT element. To collect the generated charges due to the piezoelectric effect, wires are connected at the sliver electrodes on both sides of the PZT elements.

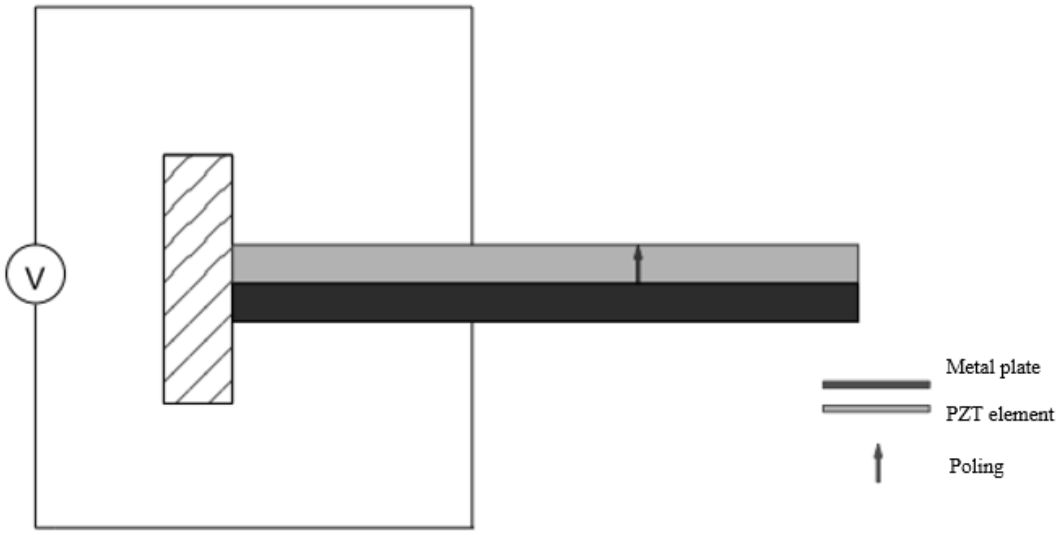

Figure 2.4 Unimorph structure sensor

When external pressure is applied, it will cause bending on both the PZT element and the metal plate. Since it is a beam structure, the deflection results from the bending of both elements. Charges are created on the electrodes and are collected by the wires. The defection is generally small compared to the thickness of the PZT element. By the small bending elastic theory, the output voltage of the sensor is proportional to the magnitude of the external pressure.

2.2.2 Bimorph Structure and Triple Layer Sensor

The bimorph structure sensor consists of two PZT plates placed on both the upper and lower sides of a beam. Since the polarization direction and connection method could be different, there are two connecting methods for the bimorph sensor, parallel and series connection (Figure 2.5).

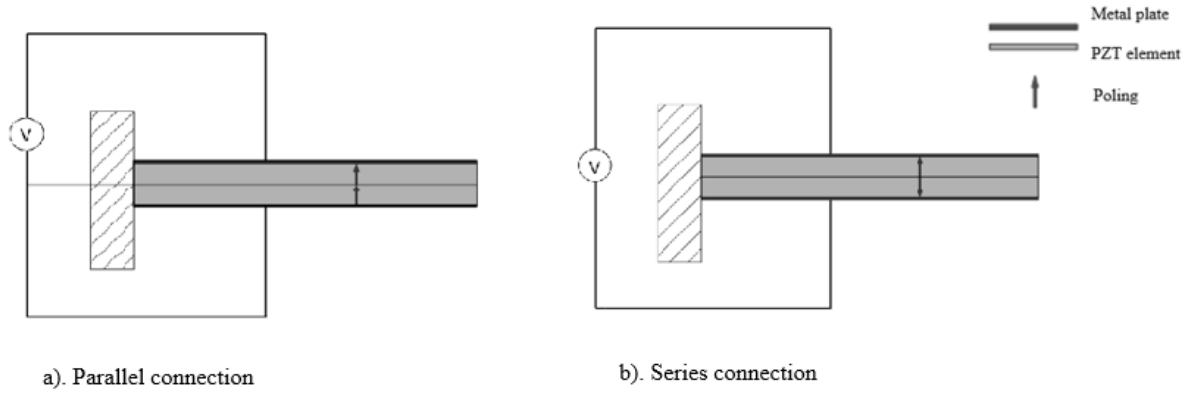

Figure 2.5 Bimorph structure sensor a) in parallel connection b)in series connection

Take a force downwards at the free end as an example to introduce how it works. Bending caused by force would create tensile stress on the upper layer and compressive stress on the bottom one in the horizontal direction. As a result, when it is in series connection, negative charges are accumulated at the top electrode and positive charges at the bottom electrode. As for the parallel connection, two PZT elements would have the same charge distribution on the electrodes. Consequently, the sensor in a parallel connection generates twice the number of charges of a series connection, whereas the voltage generated is half of the value by a series connection. The reason why is the capacitance of two identical pieces of the capacitor in the parallel configuration is four

times larger than in series connection. The result could be proved by the formula of voltage across the capacitor $V = \frac{Q}{C}$.

Two kinds of connection methods could both canceled the pyroelectric effect. From the performance of the voltage generation, the series connection sensor should be preferred. However, the parallel connection is selected because it generates a more stable signal when exposed to external load [15].

One more special case is the triple layer bender which prevents the PZT be broken from the vibration. It contains two PZT elements on both sides of the additional metal plate (Figure 2.6). The PZT elements could also be connected in series or parallel connections like bimorph structure. For the sensor in this thesis, the triple layer structure is selected to build the accelerometer.

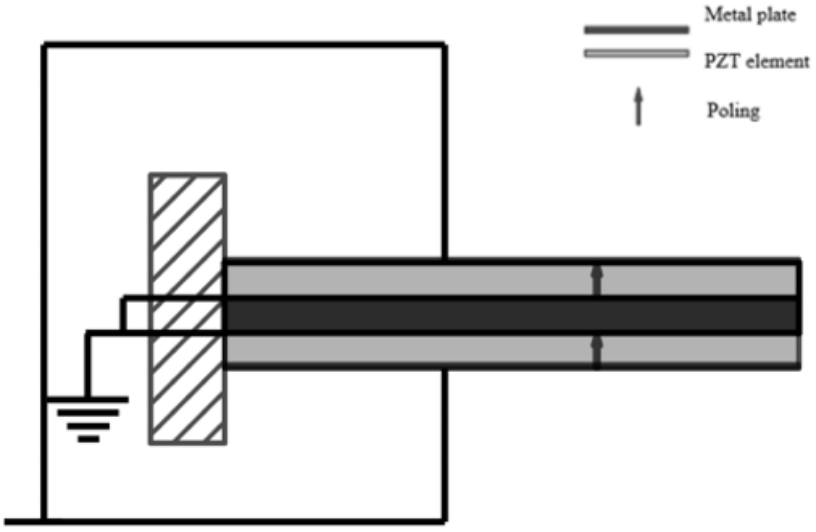

Figure 2.6 Triple layer structure sensor

The parallel connection that the respective opposing surface of two upper/lower bonded sheets are connected to serve as a signal take-out electrode and the bonded surface electrode is also used as a signal take-out electrode. Considering the direction of the thermal effect with the

assumption that the temperature is rising, it would arise a voltage difference that has the opposite direction of the polarization. During a clockwise bending process for parallel configuration, the voltage generation is in the same direction as the polarization on the top surface and the negative direction of the polarization on the bottom surface. Thus, the thermal effect decreases the value of the voltage generated on the top surface and increases the value on the bottom surface, and they are canceled mutually. However, the heat conduction in the PZT material is not uniform, so the temperature effect cancellation might not be useful under critical temperature. It is also impossible to make the output the same at different temperatures.

2.3 Theoretical Analysis of The Sensor

2.3.1 Static Response Analysis

This part is mainly navigated by the work from Wang and Smits [16], [17]. Before the calculation, one thing that should be noticed is that for sign convection. The calculation is based on the situation that the positive voltage is connected to the upper element and the negative one to the lower surface. During the derivation, the element is set in series connection. Therefore, the electric field has the same direction with the polarization in the lower element and reverse direction with polarization in the upper element. Under this assumption, for series connection, the constitutive equations for the upper element with electric field are:

$$S_1{}^U = s^E{}_{11} T^U{}_1 - d_{31} E_3 \tag{2.1}$$

$$D_3{}^U = -d_{31} T^U{}_1 + \varepsilon^T{}_{33} E_3 \tag{2.2}$$

The lower element only gives the piezoelectric element a negative sign and it becomes:

$$S_1{}^L = s^E{}_{11}T^L{}_1 + d_{31}E_3 \tag{2.3}$$

$$D_3{}^L = d_{31}T^L{}_1 + \varepsilon^T{}_{33}E_3 \tag{2.4}$$

For beam element, which is non-piezoelectric, the equation is:

$$S_1{}^M = s^M{}_{11}T^M{}_1 \tag{2.5}$$

The energy method is used to conduct the relationship between independent and dependent variables under different situations. For further discussion, the energy equation must be introduced. The energy density u of the element is given:

$$u = \frac{1}{2}ST + \frac{1}{2}DE \tag{2.6}$$

Substitution equation (2.1) and (2.2) into the energy density equation to get the upper element density u^U:

$$u^U = \frac{1}{2}s^E{}_{11}(T^U{}_1)^2 - d_{31}E_3T^U{}_1 + \frac{1}{2}\varepsilon^T{}_{33}E_3{}^2 \tag{2.7}$$

And substitution equation (2.3) and (2.4) for the lower element:

$$u^L = \frac{1}{2}s^E{}_{11}(T^L{}_1)^2 + d_{31}E_3T^L{}_1 + \frac{1}{2}\varepsilon^T{}_{33}E_3{}^2 \tag{2.8}$$

By the same method, the energy for beam element could be written as:

$$u^M = \frac{1}{2}s^M{}_{11}(T^M{}_1)^2 \tag{2.9}$$

The total energy in the piezoelectric bimorph structure sensor could be integrated from the density as:

$$U = \iiint (u^L + u^M + u^U)dxdydz \tag{2.10}$$

The boundary of integration is 0 to length L in the x-direction, 0 to width w in the y-direction, and thickness of the PZT element in the z-direction. The total energy is the sum of the upper, medium, and lower energy u^U, u^U, and u^L.

2.3.1.1 Free Bender

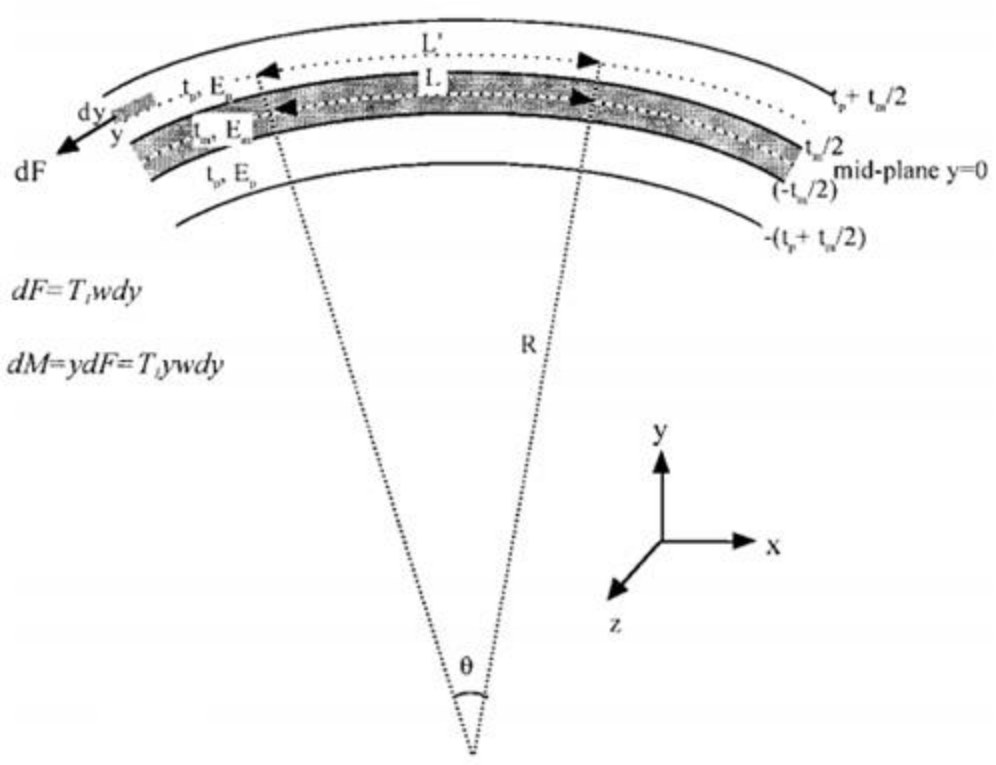

Figure 2.7 Beam element under bending [17]

The first step is to analyze the free bender and then extend the conclusion to other specific external input. Since the structure is symmetrical, the natural plane of the entire structure is at the midplane. Consequently, no extensional strain appears in the midplane. So, there is a continuity among the structure, the stain at the contact surface of all the elements must be the same, and it is zero at the midplane and reaches the maximum at the top as well as the bottom surface.

The radius of curvature is the same for both elements and it could be expressed as:

$$\kappa = \frac{d^2 v}{dx^2} = \frac{1}{R} \tag{2.11}$$

where v is the vertical displacement of the midplane. As a result, the extensional strain could be expressed as:

$$S_1 = \frac{L' - L}{L} = \frac{(R + y)\theta - R\theta}{R\theta} = \frac{y}{R} = \kappa y \tag{2.12}$$

The assumption of a perfect joint beam is made, so the radii of the curvature of both elements are equal. The subscript could be dropped and S_1 is the same for all elements.

Substituting equation (2.11) back to equation (2.1) and (2.3):

$$\kappa y = s^E{}_{11} T^U{}_1 - d_{31} E_3 \tag{2.13}$$

$$\kappa y = s^E{}_{11} T^L{}_1 + d_{31} E_3 \tag{2.14}$$

And rearrange it by leaving the term *T* on the left side:

$$T^U{}_1 = \frac{1}{s^E{}_{11}} (\kappa y) + \frac{1}{s^E{}_{11}} d_{31} E_3 \tag{2.15}$$

$$T^U{}_1 = \frac{1}{s^E{}_{11}} (\kappa y) - \frac{1}{s^E{}_{11}} d_{31} E_3 \tag{2.16}$$

As for the beam element, which is non-piezoelectric, the term of the piezoelectric constant should be neglected:

$$T^M{}_1 = \frac{1}{s^M{}_{11}} (\kappa y) \tag{2.17}$$

All terms of the equation (2.6) and equation (2.7) are known so that it could be written as:

$$u^U = \frac{1}{2} \frac{1}{s^E{}_{11}} \left((\kappa y) + d_{31} E_3 \right)^2 - \frac{1}{s^E{}_{11}} d_{31} E_3 ((\kappa y) + d_{31} E_3) + \frac{1}{2} \varepsilon^T{}_{33} {E_3}^2 \tag{2.18}$$

$$\frac{t_m}{2} \leq y \leq \frac{t_m}{2} + t_p$$

$$u^L = \frac{1}{2}\frac{1}{{s^E}_{11}}\left((\kappa y) - d_{31}E_3\right)^2 + \frac{1}{{s^E}_{11}}d_{31}E_3\left((\kappa y) - d_{31}E_3\right) + \frac{1}{2}{\varepsilon^T}_{33}{E_3}^2 \quad (2.19)$$

$$-\left(\frac{t_m}{2} + t_p\right) \le y \le -\frac{t_m}{2}$$

Simplified the equation (2.17) and equation (2.18):

$$u^U = u^L = \frac{1}{2}\left(\frac{1}{{s^E}_{11}}(\kappa y)^2 - \frac{1}{{s^E}_{11}}(d_{31}E_3)^2 + {\varepsilon^T}_{33}{E_3}^2\right) \quad (2.20)$$

$$-\left(\frac{t_m}{2} + t_p\right) \le y \le -\frac{t_m}{2}, \frac{t_m}{2} \le y \le \frac{t_m}{2} + t_p$$

The result shows the energy density in the upper layer is the same as the lower layer. It is easy to explain this situation because the magnitude of the moment and electric field is the same, and the direction could not influence the energy accumulation.

One more step to get the total energy is to find the energy in the beam element which the density is:

$$u^M = \frac{1}{2}\frac{1}{{s^M}_{11}}(\kappa y)^2 \quad (2.21)$$

$$-\frac{t_m}{2} \le y \le \frac{t_m}{2}$$

Integrated all the energy density and add together, the total energy could be calculated:

$$U^U = \int_0^L \int_0^w \int_{\frac{t_m}{2}}^{\frac{t_m}{2}+t_p} \left(\frac{1}{2}\left(\frac{1}{{s^E}_{11}}(\kappa y)^2 - \frac{1}{{s^E}_{11}}(d_{31}E_3)^2 + {\varepsilon^T}_{33}{E_3}^2\right)\right) dxdydz$$

$$= \frac{1}{2}\int_0^L \int_0^w \left[\frac{1}{12}\frac{1}{{s^E}_{11}}\kappa^2\left(3{t_m}^2 t_p + 6t_m{t_p}^2 + 4{t_p}^3\right) + \left({\varepsilon^T}_{33} - \frac{1}{{s^E}_{11}}\right){E_3}^2 t_p\right] dxdz \quad (2.22)$$

$$U^L = \int_0^L \int_0^w \int_{-\left(\frac{t_m}{2}+t_p\right)}^{-\frac{t_m}{2}} \left(\frac{1}{2}\left(\frac{1}{{s^E}_{11}}(\kappa y)^2 - \frac{1}{{s^E}_{11}}(d_{31}E_3)^2 + {\varepsilon^T}_{33}{E_3}^2\right)\right) dxdydz$$

$$= \frac{1}{2}\int_0^L \int_0^w \left[\frac{1}{12}\frac{1}{{s^E}_{11}}\kappa^2\left(3{t_m}^2 t_p + 6t_m{t_p}^2 + 4{t_p}^3\right) + \left({\varepsilon^T}_{33} - \frac{1}{{s^E}_{11}}\right){E_3}^2 t_p\right] dxdz \quad (2.23)$$

$$U^M = \int_0^L \int_0^w \int_{-\frac{t_m}{2}}^{\frac{t_m}{2}} \frac{1}{2} \frac{1}{{s^E}_{11}} (\kappa y)^2 dx dy dz = \int_0^L \int_0^w \frac{Lw}{24} \frac{1}{{s^M}_{11}} \kappa^2 {t_m}^3 dx dz \qquad (2.24)$$

$$U = \frac{1}{12} \int_0^L \int_0^w \left[\frac{1}{{s^E}_{11}} \kappa^2 \left(3{t_m}^2 t_p + 6 t_m {t_p}^2 + 4{t_p}^3\right) + 12 \left({\varepsilon^T}_{33} - \frac{1}{{s^E}_{11}} {d_{31}}^2 \right) {E_3}^2 t_p \right.$$

$$\left. + \frac{1}{2} \frac{1}{{s^M}_{11}} \kappa^2 {t_m}^3 \right] dx dz$$

$$= \frac{1}{24} \int_0^L \int_0^w \left[\frac{1}{{s^E}_{11}} \frac{1}{{s^M}_{11}} D\kappa^2 + 24 \left({\varepsilon^T}_{33} \frac{1}{{s^E}_{11}} {d_{31}}^2 \right) {E_3}^2 t_p \right] dx dz \qquad (2.25)$$

where $D = 2{s^M}_{11}\left(3{t_m}^2 t_p + 6 t_m {t_p}^2 + 4{t_p}^3\right) + {s^M}_{11} {t_m}^3$. The equation could be applied to other situation rather than free bending by adjusting the expression of the curvature κ . In this thesis, the sensor to generate the voltage is desired, so the situation of external voltage V moment M, Force F, and pressure p would be discussed with respect to the charge generated.

2.3.1.2 External Voltage

Taking the external voltage into consideration. Its influence on the curvature is the thing needed to calculate the change of the energy. Checking the Figure 2.7, for the elementary area dA, the elementary moment dM generated by the elastic force dF normal to dA could be calculated by:

$$dM = y dF \qquad (2.26)$$

To related it with the known variable, the force could be expressed by the normal stress T_1 as:

$$dF = T_1 dA \qquad (2.27)$$

where $dA = w dy$.Subsequently, the moment could be rewritten as:

$$dM = T_1 w dy \qquad (2.28)$$

Integrated both side of the equation (2.26):

$$M = \int_{-\left(\frac{t_m}{2}+t_p\right)}^{-\frac{t_m}{2}} \left(\frac{1}{s^E{}_{11}}(\kappa y) - \frac{1}{s^E{}_{11}} d_{31} E_3\right) w y dy + \int_{-\frac{t_m}{2}}^{\frac{t_m}{2}} \left(\frac{1}{s^M{}_{11}} \kappa y^2\right) w dy + \int_{\frac{t_m}{2}}^{\frac{t_m}{2}+t_p} \left(\frac{1}{s^E{}_{11}}(\kappa y) + \frac{1}{s^E{}_{11}} d_{31} E_3\right) w y dy \quad (2.29)$$

After simplification, it becomes:

$$12 s^M{}_{11} s^E{}_{11} M = \kappa w D - 12 w s^M{}_{11} d_{31} E_3 \left(t_m t_p + {t_p}^2\right) \quad (2.30)$$

Since the external moment is equal to zero, the curvature becomes:

$$\kappa = \frac{12 w s^M{}_{11} d_{31} E_3 \left(t_m t_p + {t_p}^2\right)}{D} \quad (2.31)$$

Substituting it back to equation (2.25) to get the total energy as:

$$U = L w t_p \varepsilon^T{}_{33} {E_3}^2 \left(1 - \frac{D - 6 s^M{}_{11} t_p \left(t_p + t_m\right)^2}{D} {k_{31}}^2\right) \quad (2.32)$$

where ${k_{31}}^2 = {d_{31}}^2 / \varepsilon^T{}_{33}\, s^E{}_{11}$. Since $E_3 = V/2t_p$, in this case, V is the voltage across the top and the bottom surface. The charge generated could be calculated by:

$$Q = \frac{\partial U}{\partial V} = \frac{L w}{2 t_p} \varepsilon^T{}_{33} \left(1 - \frac{D - 6 s^M{}_{11} t_p \left(t_p + t_m\right)^2}{D} {k_{31}}^2\right) V \quad (2.33)$$

2.3.1.3 External Moment and Voltage

The moment is applied to provide a rotation or angular deflection to the beam structure. To detect the moment, the relationship between the moment and the charge generated is the point to be concerned about. The moment M is set at the free end of the beam. Review the equation (2.30), when the M is no longer zero, the curvature could be expressed as:

$$\kappa = \frac{12 w s^M{}_{11} s^E{}_{11} M}{D w} + \frac{12 s^M{}_{11} d_{31} E_3 \left(t_m t_p + {t_p}^2\right)}{D} \quad (2.34)$$

Substituting the curvature back to equation (2.23) to get the energy equation:

$$U = \frac{6Ls^M{}_{11}s^E{}_{11}M^2}{Dw} + \frac{12Ls^M{}_{11}d_{31}E_3\left(t_m t_p + {t_p}^2\right)M}{D} + Lwt_p\varepsilon^T{}_{33}{E_3}^2\left(1 - \frac{D - 6s^M{}_{11}t_p\left(t_p + t_m\right)^2}{D}{k_{31}}^2\right) \quad (2.35)$$

Compared with equation (2.32), energy generated under an additional moment gets two more extra terms contains moment. When the voltage is 0, only the first term would remain. While the bending moment becomes 0, the internal energy would be the same as the equation (2.32).

Taking the derivative with respect to voltage, the charge generated in the triple layer bender could be found in the triple layer bender as:

$$Q = \frac{\partial U}{\partial V} = \frac{6s^M{}_{11}d_{31}(t_m + t_p)L}{D}M + \frac{Lw}{2t_p}\varepsilon^T{}_{33}\left(1 - \frac{D - 6s^M{}_{11}t_p\left(t_p + t_m\right)^2}{D}{k_{31}}^2\right)V \quad (2.36)$$

2.3.1.4 External Force and Voltage

The piezoelectric force sensor is a common application for the PZT cantilever beam structure sensor. Therefore, it is essential to discover how the force changes the internal variables. Force applied would cause a tip displacement, and the energy method could analyze the change numerically.

An external force is applied at the free end of the beam and perpendicular to it. The moment at any position of the length of the beam x caused by force is:

$$M = F(L - x) \quad (2.37)$$

Therefore, replaced the term in the equation (2.28), the curvature of the beam under the external force and voltage now becomes:

$$\kappa = \frac{12ws^M{}_{11}s^E{}_{11}F(L - x)}{Dw} + \frac{12s^M{}_{11}d_{31}E_3\left(t_m t_p + {t_p}^2\right)}{D} \quad (2.38)$$

Substituting it to the equation (2.23) to find the total internal energy of the triple layer beam under the effect of the voltage and force as:

$$U = \frac{2{s^M}_{11}{s^E}_{11}L^3F^2}{Dw} + \frac{6{s^M}_{11}d_{31}E_3\left(t_m t_p + {t_p}^2\right)L^2F}{D} + Lwt_p{\varepsilon^T}_{33}{E_3}^2\left(1 - \frac{D - 6{s^M}_{11}t_p\left(t_p + t_m\right)^2}{D}{k_{31}}^2\right) \quad (2.39)$$

Since it is just a replacement for M with the expression of F, the result is similar to the energy equation of the external moment. The first and second term is obtained by the presence of the external force. In the situation $F = 0$, the energy would be the same as the equation (2.32).

The charge generated by the external force is:

$$Q = \frac{\partial U}{\partial V} = \frac{3{s^M}_{11}d_{31}(t_m + t_p)L^2}{D}F + \frac{Lw}{2t_p}{\varepsilon^T}_{33}\left(1 - \frac{D - 6{s^M}_{11}t_p\left(t_p + t_m\right)^2}{D}{k_{31}}^2\right)V \quad (2.40)$$

2.3.1.5 External Pressure and Voltage

Pressure sensors are usually designed in the shape of disk. However, a beam structure accelerometer is customary. The vibration brings inertial body force, which could be equivalent to surface load. Processing the same procedure as an external force, first finding the expression of moment M caused by pressure and substituting it into κ to find the energy equation:

$$M = \frac{1}{2}pw(L - x)^2 \quad (2.41)$$

Substituting into equation (2.30):

$$\kappa = \frac{6w{s^M}_{11}{s^E}_{11}p(L - x)^2}{Dw} + \frac{12{s^M}_{11}d_{31}E_3\left(t_m t_p + {t_p}^2\right)}{D} \quad (2.42)$$

Like the process before, substituting it back to energy equation and the energy under the external pressure and voltage could be expressed as:

$$U = \frac{3ws^{M}{}_{11}s^{E}{}_{11}L^5p^2}{10Dw} + \frac{2ws^{M}{}_{11}d_{31}E_3\left(t_m t_p + {t_p}^2\right)L^3p}{D} + Lwt_p\varepsilon^{T}{}_{33}{E_3}^2\left(1 - \frac{D - 6s^{M}{}_{11}t_p\left(t_p + t_m\right)^2}{D}{k_{31}}^2\right) \quad (2.43)$$

Since it is just a replacement for p with the expression of F, the result is similar to the energy equation of the external moment. The first and second term is obtained by the presence of the external pressure. In the situation $p = 0$, the energy would be the same as the equation (2.32).

The charge generated could be calculated as:

$$Q = \frac{\partial U}{\partial V} = \frac{ws^{M}{}_{11}d_{31}(t_m + t_p)L^5}{D}p + \frac{Lw}{2t_p}\varepsilon^{T}{}_{33}\left(1 - \frac{D - 6s^{M}{}_{11}t_p\left(t_p + t_m\right)^2}{D}{k_{31}}^2\right)V \quad (2.44)$$

2.3.1.6 General Solution

The sections all above conclude the result that contains the charge generated Q with different external variables: M, F, p, V. Those relationships help with the analysis of the theoretical sensitivity for different types of sensors. As the results imply, the charge generated by different external variables is independent of each other. It is reasonable to conclude a result by superposition method, the constitutive equation with respect to charge Q for series connection bimorph is:

$$Q = \frac{6s^{M}{}_{11}d_{31}\left(t_m + t_p\right)L}{D}M + \frac{3s^{M}{}_{11}d_{31}\left(t_m + t_p\right)L^2}{D}F + \frac{ws^{M}{}_{11}d_{31}\left(t_m + t_p\right)L^3}{D}p + \frac{Lw}{2t_p}\varepsilon^{T}{}_{33}\left(1 - \frac{D - 6s^{M}{}_{11}t_p\left(t_p + t_m\right)^2}{D}{k_{31}}^2\right)V \quad (2.45)$$

For parallel connection, the equation could be by change some constants in the equation of series connection. First, the piezoelectric coefficients are doubled since the strength of the electric is twice in parallel connection than the series connection. Moreover, the dielectric term in parallel

connection is quadrupled because the capacitance is four times larger than the series configuration. The equation for charges Q in the parallel configuration is:

$$Q = \frac{12s^{M}{}_{11}d_{31}(t_m + t_p)L}{D}M + \frac{6s^{M}{}_{11}d_{31}(t_m + t_p)L^2}{D}F + \frac{2ws^{M}{}_{11}d_{31}(t_m + t_p)L^3}{D}p + \frac{2Lw}{t_p}\varepsilon^{T}{}_{33}\left(1 - \frac{D - 6s^{M}{}_{11}t_p(t_p + t_m)^2}{D}k_{31}{}^2\right)V \quad (2.46)$$

When the parallel configuration sensor is working as a pressure sensor, the condition of the external variables is $F = M = V = 0$, so the charge generated become:

$$Q = \frac{2ws^{M}{}_{11}d_{31}(t_m + t_p)L^3}{D}p \quad (2.47)$$

The open circuit voltage between two elements is expressed as:

$$V = \frac{Q}{C} \quad (2.48)$$

In equation (2.48), C is the total capacitance of the sensor. It could be calculated by:

$$C = \frac{\partial Q}{\partial V} = \frac{2Lw}{t_p}\varepsilon^{T}{}_{33}\left(1 - \frac{D - 6s^{M}{}_{11}t_p(t_p + t_m)^2}{D}k_{31}{}^2\right) \quad (2.49)$$

Substituting back into equation (2.48), the equation is processed as:

$$V = \frac{Q}{C} = \frac{2ws^{M}{}_{11}d_{31}(t_m + t_p)L^3}{D}p \Big/ \frac{2Lw}{t_p}\varepsilon^{T}{}_{33}\left(1 - \frac{D - 6s^{M}{}_{11}t_p(t_p + t_m)^2}{D}k_{31}{}^2\right) \quad (2.50)$$

To have a more apparent expression, two factors A and B are defined as:

$$A = \frac{s^{E}{}_{11}}{s^{M}{}_{11}}, B = \frac{t_m}{2t_p} \quad (2.51)$$

where $s^{E}{}_{11}$ and $s^{M}{}_{11}$ are the modulus of the elastic for beam and the piezoelectric element. Therefore, A is the ratio for Young's modulus, and B is the thickness ratio of the beam and PZT element. The equation (2.51) becomes:

$$V = \frac{Q}{C} = \frac{d_{31}L^2}{2\varepsilon^T{}_{33}t_p} \times \frac{(2B+1)}{4\left(1-k_{31}{}^2\right)(AB^3+3B^2+3B+1)+3k_{31}{}^2(2B+1)^2}p \qquad (2.52)$$

To have a high sensitivity, the sensor should be fabricated by materials with a high ratio of $\frac{d_{31}}{\varepsilon^T{}_{33}}$ and high electromechanical constant k_{31}.

2.3.2 Dynamic Response

The static load response was discussed in the previous section. However, when it works as an accelerometer, the vibration would arise a dynamic load. Laboratory vibrator usually takes a sinusoidal function $u(t) = U_0\omega^2 \sin(\omega t)$ as input at the fixed end.

To analyze the output with dynamic load, it is necessary to check back the strain equation. The average strain in the layer is defined as:

$$\bar{S_1}(x,t) = \frac{1}{t_{layer}} \int S_1(x,z)dz = \frac{\frac{1}{2}\left(t_m + t_p\right)}{R(x,t)} \qquad (2.53)$$

Since no external voltage is applied, substituting the equation (2.53) back to equation (2.1) and it becomes:

$$T_1 = \frac{1}{S^E{}_{11}}\bar{S_1}(x,t) \qquad (2.54)$$

Then substituting it to equation (2.2) to get the charge density D as:

$$D_3 = \frac{d_{31}}{s^E{}_{11}}\bar{S_1}(x,t) \qquad (2.55)$$

The total charge generated on both electrodes in parallel connection could be calculated by integrated the charge density over the area as:

$$Q = 2\int_A D_3\, dA = 2\int_0^l \frac{\frac{1}{2}\left(t_m + t_p\right)}{R(x,t)} \frac{2d_{31}}{s^E{}_{11}} w dx = 2\int_0^l \frac{\left(t_m + t_p\right)}{R(x,t)} \frac{d_{31}}{s^E{}_{11}} w dx \qquad (2.56)$$

To relate the $R(x,t)$ to the vertical displacement $y(x,t)$, the assumption that the small deflection of the bending is made. As a result, an equation could be built like:

$$\frac{1}{R(x,t)} = \frac{d\theta}{dL} \approx \frac{d\theta}{dx} = \frac{\partial^2 y(x,t)}{\partial x^2} \tag{2.57}$$

Therefore, the equation (2.56) could be rewritten as:

$$Q = \int_A D_3 \, dA = 2\left(t_m + t_p\right) \frac{d_{31}}{s^E{}_{11}} w \int_0^l \frac{\partial^2 y(x,t)}{\partial x^2} dx \tag{2.58}$$

To solve the Q, the partial differential equation about y should be solved.

The standard beam motion formula with sinusoidal excitation $U(t) = U_0 \sin(\omega t)$ at the fixed end could be written as:

$$c^2 \frac{\partial^4 y(x,t)}{\partial x^4} + \frac{\partial^2 y(x,t)}{\partial x^2} = U_0 \omega^2 \sin(\omega t) \tag{2.59}$$

where $c = \sqrt{\frac{EI}{\rho w(t_m+2t_p)}}$, $y(x,t)$ is the displacement at the vertical direction, ρ is the density of the triple layer structure, and H is the height of the entire element. The partial differential equation (2.59) could be solved based on the modal function. The solution is the product form of a spatial characteristic function $\phi_i(x)$ and a time-dependent function $q_i(t)$. The linear superposition of all modal function is the solution of the differential equation and it could be expressed as [18]:

$$y_p(x,t) = \sum_{n=1}^{\infty} \phi_n(x) q_n(t) \tag{2.60}$$

where

$$\phi_n(x) = C_{1n}[(cos\beta_n x - cosh\beta_n x) - (sin\beta_n x - sinh\beta_n x)]$$

For the function $q_n(t)$, it is the convolution of the input force and impulse response of the bimorph, which could be written as:

$$q_n(t) = \int_0^t P_n(t-\gamma)\, h(t) d\gamma \tag{2.61}$$

where

$P_n = \int_0^L U_0 \sin(\omega t)\phi_n(x)dx$

$h(t) = \frac{2}{\omega_n L} sin(\omega_n t)$

$\omega_n = \beta_n L^2 (\frac{EI}{\rho A L^4})^{\frac{1}{2}}$

A is the area of the bimorph.

Substituting the equation (2.60) into equation (2.58), the results could be conducted with Jung's work to calculate the value of $\int_0^l \frac{\partial^2 y(x,t)}{\partial x^2} dx$ as [19]:

$$\begin{aligned} Q = 2(t_m + t_p)\frac{d_{31}}{s^E{}_{11}} w \sum_{n=1}^{\infty} C_{1n}\beta_n[-(sin\beta_n L + sinh\beta_n L) - K_{rn}(cos\beta_n L + cosh\beta_n L)] \\ \times \frac{2U_0 C_{1n}}{L\beta_n}[sin\beta_n L - sinh\beta_n L + K_{rn}(cos\beta_n L + cosh\beta_n L) - 2K_{rn}] \\ \times \left\{ sin\omega_n t \left[\frac{1-\cos(\omega-\omega_n)\, t}{2(\omega-\omega_n)} + \frac{1-\cos(\omega+\omega_n)\, t}{2(\omega+\omega_n)} \right] \right. \\ \left. - cos\omega_n t \left[\frac{\sin(\omega-\omega_n)\, t}{2(\omega-\omega_n)} - \frac{\sin(\omega+\omega_n)\, t}{2(\omega-\omega_n)} \right] \right\} \end{aligned} \tag{2.62}$$

$C_{1n} = 0.707$

$K_{rn} = \frac{cos\beta_n L + cosh\beta_n L}{sin\beta_n L + sinh\beta_n L}$

With equation (2.62), the output charges could be calculated when the force amplitude U_0 and the force frequency ω are known.

2.3.3 Frequency Analysis

The result in section 2.3.2 indicates that the frequency could influence the output voltage under dynamic load. As mentioned in the previous section, only a limited range of frequency for the sensor generates the output with the same sensitivity. Otherwise, the sensitivity varies with the frequency. To find the usage frequency of the sensor, the mechanical vibration of the sensor should be discussed. The behavior of the sensor could also be treated as a mass vibration system with a damper and spring. The structure is shown in Figure 2.8.

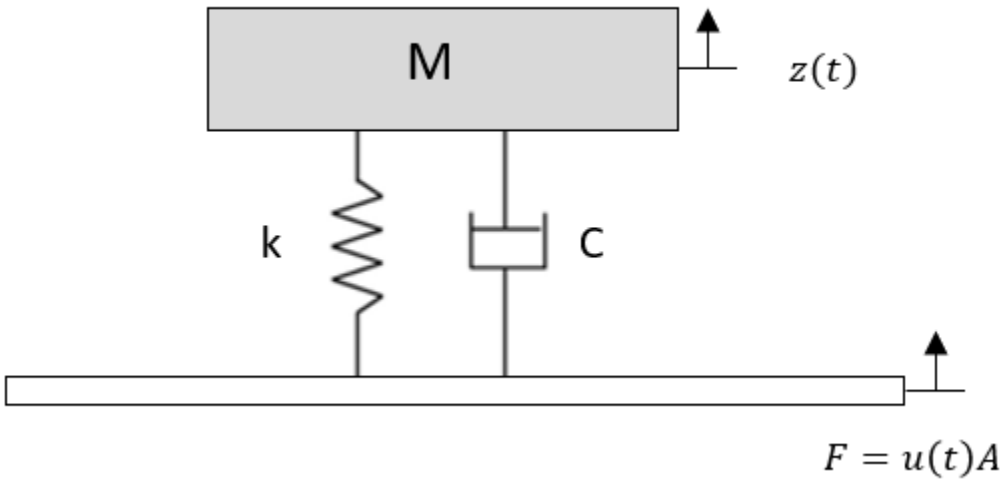

Figure 2.8 The mechanical model of the sensor

The basement of the structure vibrated in stress $u(t) = U_0 sin\omega$ which gives uniform stress on the surface. Therefore, the force on the surface of the sensor is $F(t) = u(t)A$, where A is the effective surface area. The govern equation could be written as:

$$m\ddot{z}(t) + c\dot{z}(t) + kz(t) = u(t)A \qquad (2.63)$$

where m is the effective mass, c is the effective damping coefficient, and k is the effective spring constant. Taking Laplace transform of the governing equation and it becomes:

$$ms^2Z + csZ + kZ = U(s)A \tag{2.64}$$

Substituting the nature frequency $\omega_n = \sqrt{\frac{k}{m}}$, damping ratio $\xi = \frac{c}{2\sqrt{km}}$, and $s = j\omega$ in the equation. The transfer function from force to displacement could be calculated as:

$$\frac{Z(s)}{U(s)A} = \frac{1}{k}\frac{{\omega_n}^2}{s^2 + 2\xi\omega_n s + {\omega_n}^2} \tag{2.65}$$

A PZT sensor could also be regarded as an equivalent circuit contains a capacitance C_p , a leakage resistance R_p, and a current source $I = dQ/dt$ (Figure 2.9).

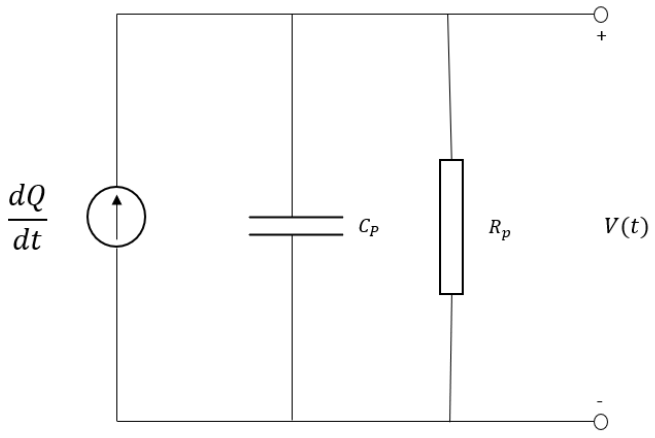

Figure 2.9 Electrical model of the sensor

The charges generated by the sensor could be expressed as:

$$Q(t) = K_q z \tag{2.66}$$

where K_q is the charge generated per unit displacement. Combined equation (2.65) and (2.66), the transfer function of force and charge generated is established in the form of:

$$\frac{Q(s)}{U(s)A} = \frac{K_q}{k} \frac{{\omega_n}^2}{s^2 + 2\xi\omega_n s + {\omega_n}^2} \tag{2.67}$$

To connect voltage and charge, Kirchhoff voltage law is applied to the circuit, and it could derive an equation:

$$\frac{dQ}{dt} = \frac{K_q dZ}{dt} = C_p \frac{dV}{dt} + \frac{V}{R_p} \tag{2.68}$$

Taking Laplace transform with the time constant $\tau = R_p C_p$ and it becomes:

$$\frac{K_q}{C_p} sZ(s) = sV(s) + \frac{V(s)}{\tau} \tag{2.69}$$

$$\frac{V(s)}{Z(s)} = \frac{K_q}{C_p} \frac{\tau s}{\tau s + 1} \tag{2.70}$$

Substituting the results in equation (2.66) to get:

$$\frac{V(s)}{U(s)} = \frac{AK_q}{C_p k} \frac{{\omega_n}^2}{s^2 + 2\xi\omega_n s + {\omega_n}^2} \frac{\tau s}{\tau s + 1} \tag{2.71}$$

The function illustrated the idea that the output voltage is frequency dependent. Figure 2.10 shows how output sensitivity $\frac{V}{F}$ changes with the frequency.

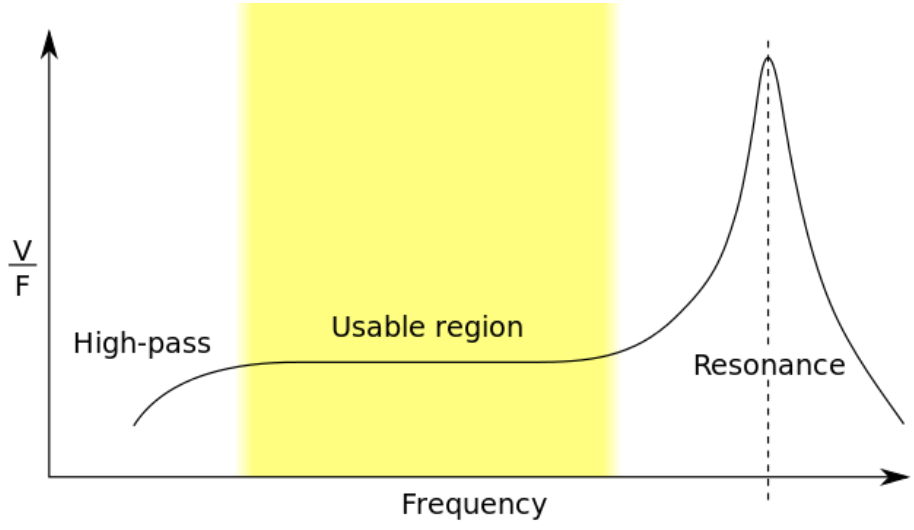

Figure 2.10 Frequency response of the sensor [20]

The usable region contains a flat line which means the frequency in this interval would not influence the sensitivity of the sensor. The upper and lower limit of the frequency should be founded. Typically, the upper limit f_U is half of the resonance frequency because the spike of the curve is due to the resonance. The lower limit of the useable region is $f_L = \frac{1}{2\pi R_p C_p}$ since the corner downward of the curve is caused by the low-frequency filtering of the resistor. The resonance frequency is determined by the mechanical properties of the sensor structure. The lower limit of frequency is dependent on the properties of the PZT materials since $R_p = \rho h_p A$ and $C_p = \frac{\varepsilon A}{h_p}$ where ρ is the resistivity, ε is the permittivity of the PZT plate. One more thing is that in parallel connection, the sensor's capacitance is doubled, and resistance is halved, so the configuration does not influence the lower limit magnitude.

3.0 Accelerometer Experiment Under Elevated Temperature

3.1 Experiment Setup

3.1.1 Design of The Beam Structure

The experiment starts with building a bimorph structure sensor in parallel configuration with PZT elements. As mentioned before, the upper limit of the operational frequency is determined by resonance frequency, which is calculated based on the beam's mechanical properties. The formula is shown in equation (3.1) as:

$$f_n = \frac{v_n}{2\pi}\sqrt{\frac{EI}{m'L^4}} \tag{3.1}$$

where v_n is depended on the motion mode of the beam. m' is the mass per unit length, which is equal to ρA, the cross-section area multiplies the density. The useable frequency should be designed as large as possible. Consequently, the beam should be short, thick, and wide to have a large resonance frequency to extend the upper limit of the working frequency.

The beam in this experiment is made from aluminum 6101. The dimension data is length $L = 7.62\ cm$, width $w = 1.91\ cm$, and thickness $h = 0.3175\ cm$. To calculate the natural frequency of the beam, the material properties of the aluminum 6101 could be discovered on the website. The modulus of elastic for aluminum is $E = 69\ GPa$, and the density of the material is $2.7\ g/cm^3$. It could be calculated by equation (3.1) that the beam natural frequency is $f_n = 446.53\ hz$. In the practical experiment, the beam is clamped to keep the length same as PZT element. It could make the actual reonaceate frequency for sensor larger than the value calculated.

3.1.2 PZT Element Preparation

The next process is to attach the PZT element (Figure 3.1) to the beam to form a bimorph structure. The first step is to check the direction of the polarization for the PZT element by d_{33} meters. The d_{33} constant could also be measured at the same time. The wrong polarization direction would cause an error in the result. Once the direction is known, the face gathering positive charges should be marked for further experimental setup. The surface collecting positive charges should be placed outside on the top surface and next to the beam on the bottom surface.

The following procedure is to attach the PZT element to the beam. Two wires need to be connected to electrodes at both sides of the elements to conduct charges. The silver conductive epoxy (MG chemicals 8831) is used to glue all the components together. One more thing is that the sliver epoxy in each layer of the element should be smeared flatly on the surface between the beam and the PZT elements to avoid the gaps that would change the reaction of the beam to the vibration. Also, it takes about 30 minutes for the sliver epoxy to be solid. It is important to wait until it dries completely, or it might be rubbed around and link the upper and lower electrodes of the PZT element, which makes it disfunction.

Figure 3.1 PZT element used in the sensor

The properties of the PZT element are put in Table 3-1. The value of d_{31} is hard to measure directly, so usually, the value is estimated to be half of the d_{33} value.

Table 3-1 Properties of PZT element

Length (cm)	5.08
Width (cm)	1.01
Thickness (cm)	0.051
Piezoelectric strain constant d_{33} $(10^{-12}C/N)$	220
Piezoelectric strain constant d_{31} $(10^{-12}C/N)$	-110
Capacitance (nF)	58
Elastic compliances constant ${s^E}_{11}$ $(10^{-12}m^2/N)$	19.23

Once the piezoelectric elements are placed on the beam correctly, the sensor could be connected to the oscilloscope to test whether there is a connection problem or not. The wires that come from the surface attached to the beam should be connected to the black ground wire, while the wire from the outer surface should be connected to the red input wire. To have an output signal, just use the finger to press the beam and check the screen to see if there is a voltage generation detected.

3.1.3 Interface Circuit Design

The number of charges generated due to the piezoelectric effect in the PZT element is small. To have the signal that can be handled by the measurement device, an interface circuit is connected to the sensor. The function of the circuit is to enlarge the voltage output by moving the charges to the capacitor in the circuit.

It is known that the PZT sensor itself could be treated as a charge source in parallel with self-resistance and self-capacitor. The interface circuit contains the sensor is shown in Figure 3.2.

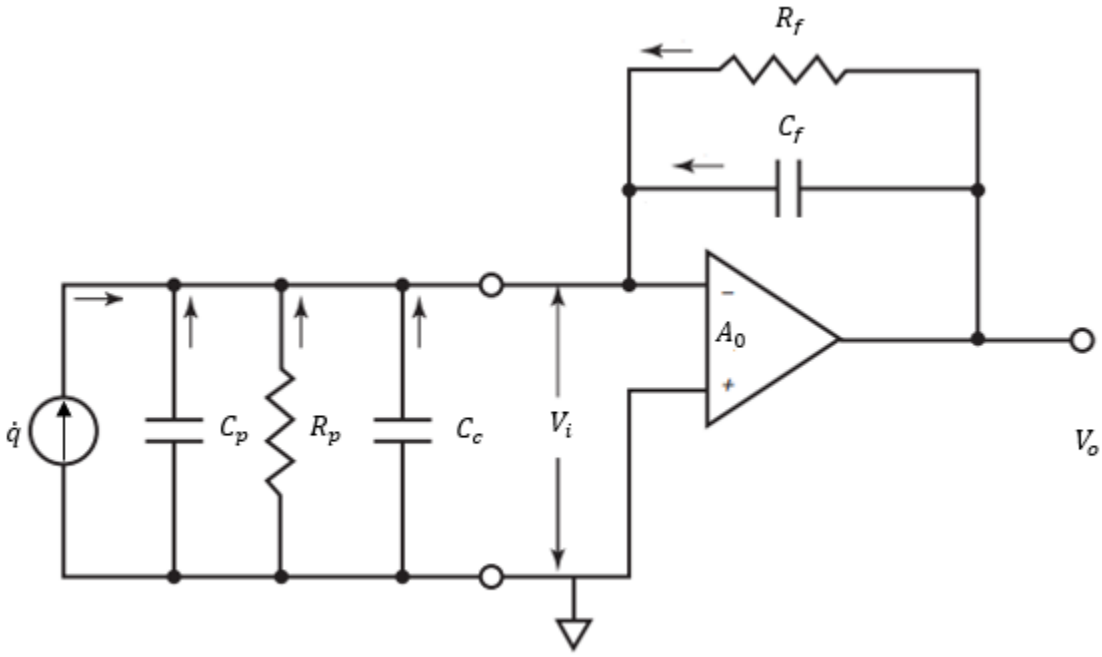

Figure 3.2 The circuit for the charge amplifier with sensor

By applying Kirchhoff current law and the assumption that the value of R_f is extremely large, the current equation for the circuit could be expressed as:

$$\dot{q} + C_P \frac{dv_0}{A_0 dt} + C_c \frac{dv_0}{A_0 dt} + C_f \left(\frac{dv_0}{dt} + \frac{dv_0}{A_0 dt}\right) + \frac{v_0 + \frac{v_0}{A_0}}{R_f} = 0 \qquad (3.2)$$

where A_0 is the gain of the open circuit amplifier, which is usually a large number. As a result, equation (3.2) could be simplified in the form of:

$$R_f C_f \frac{dv_0}{dt} + v_o = -R_f \frac{dq}{dt} \qquad (3.3)$$

To get the transfer function of the circuit, taking Laplace transform for both side of the equation and it becomes:

$$R_f C_f s V_0(s) + V_o(s) = -R_f Q(s) \tag{3.4}$$

Rearranging the equation and put the ratio of $\frac{V_0(s)}{Q(s)}$ at one side, the equation becomes:

$$\frac{V_o(s)}{Q(s)} = -R_f \frac{s}{R_f C_f s + 1} \tag{3.5}$$

Transform it into the frequency domain by substituting $s = j\omega$:

$$\frac{V_o(j\omega)}{Q(j\omega)} = -\frac{R_f j\omega}{R_f C_f j\omega + 1} \tag{3.6}$$

The time constant τ is the parameter characterizing the response a step input of a first-order, linear time-invariant system [21]. In the RC circuit, it determines how fast the system is responding to the input signal. For the charge amplifier connected in the interface circuit, the time constant could be expressed as:

$$\tau_c = R_f C_f \tag{3.7}$$

Replace $R_f C_f$ with the time constant τ in equation (3.6), the transfer function becomes:

$$G(j\omega) = \frac{\tau_c j\omega}{\tau_c j\omega + 1} \tag{3.8}$$

The magnitude of the transfer function is:

$$M = \frac{\tau_c \omega}{\sqrt{\tau_c^2 \omega^2 + 1}} \tag{3.9}$$

The measurement accuracy is depended on the magnitude of the transfer function. When $M = 1$ which requires the frequency is infinite, the sensor error is 0. It is impossible for a practical experiment. Therefore, a desired magnitude close to 1 is chosen to be placed in the equation to determine the value of the time constant. Leaving the time constant at one side of the equation (3.9) and it could be written as:

$$\tau_c > \frac{M_0}{\omega\sqrt{1 - M_0^2}} \tag{3.10}$$

It could be a reference to select the resistor and capacitor in the interface circuit but not the only one. Back to the transfer function equation (3.6) and rearrange it as:

$$\frac{V_o(j\omega)}{Q(j\omega)} = -\frac{1}{C_f\left(1+\frac{1}{C_f R_f j\omega}\right)} \tag{3.11}$$

It can be shown that this equation has a frequency response as a high pass filter with a frequency conner at:

$$f_L = \frac{1}{2\pi C_f R_f} = \frac{1}{2\pi\tau} \tag{3.12}$$

This value is the lower limit frequency of the accelerometer connected to an interface circuit. It should be as small as possible, which implied the time constant should be large.

Referring to the assumption that R_f is large enough, the transfer function could also be rewritten as:

$$\frac{V_o(j\omega)}{Q(j\omega)} = -\frac{1}{C_f} \tag{3.13}$$

which indicates that the output voltage is determined by the capacitance of the capacitor. To enlarge the output signal sensor, C_f should pick a small value.

In conclusion, to get an ideal output signal, the resistor R_f should be large enough to keep the charge flow through it at a low level. The capacitance of C_f should be small. However, a high output (small capacitance C_f) conflicts with a broad operational frequency (small lower limit of frequency means a large capacitance C_f). For good performance, it needs to make a compromise. Value of C_f must ensure the time constant is high enough to keep the output accurate, as well as the lower limit of the usable frequency is wide to fit the working environment. In this thesis, the capacitor is chosen to be $C_f = 33\ nF$ and the resistor is $R_f = 1\ M\Omega$. The magnitude of transfer function M_0 is set to be 0.95. Then, substituting the value back to equation (3.10) and (3.12) to get:

$$f_L = \frac{1}{2\pi C_f R_f} = \frac{1}{2\pi\tau} = 4.82\ Hz \tag{3.14}$$

$$\tau_c = 0.03 > \frac{M_0}{\omega\sqrt{1 - M_0^2}} = 0.0024 \tag{3.15}$$

The value of resistor and capacitor fits the requirement for frequency and accuracy for the acceleration measurement. The practical charge amplifier circuit is then built on the breadboard (Figure 3.3) based on Figure 3.2. The type of the amplifier is OP177.

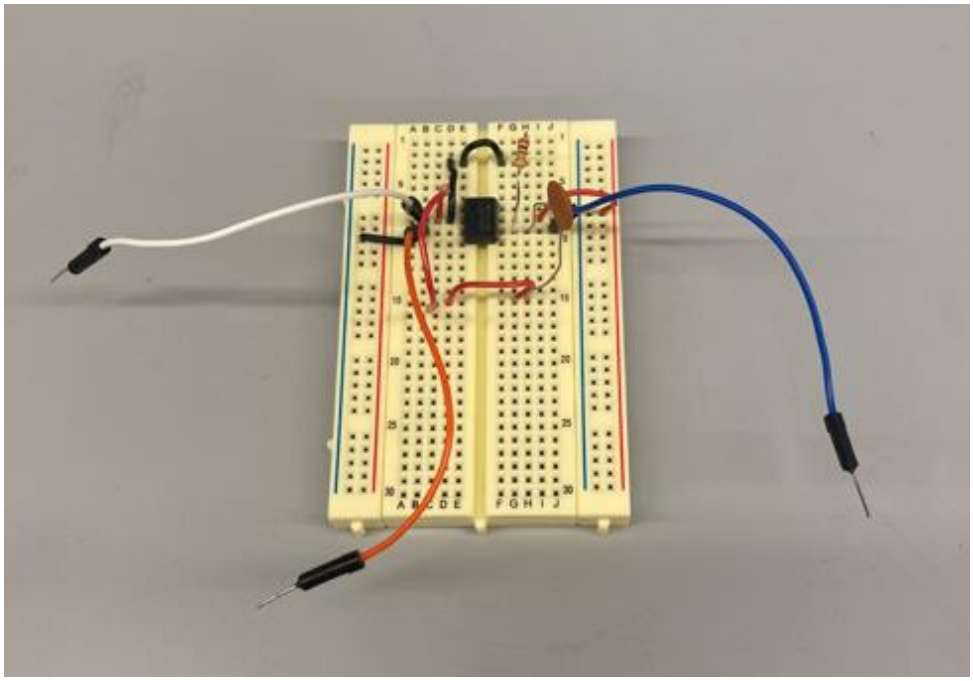

Figure 3.3 Practical charge amplifier

3.2 Equipment in The Experiment and Procedure

This section is the explanation of the experiment procedure and equipment setup. The experiment is about the temperature effect cancellation for the piezoelectric sensor. The temperature gradient is selected to be 5℃. Totally four different temperatures 25℃, 30℃, 35℃,

and 40℃ are picked to test the sensor endurability of the thermal effect. To have an environment with controllable temperature, the chamber (Model 5506-11 ets) shown in Figure 3.4 is used.

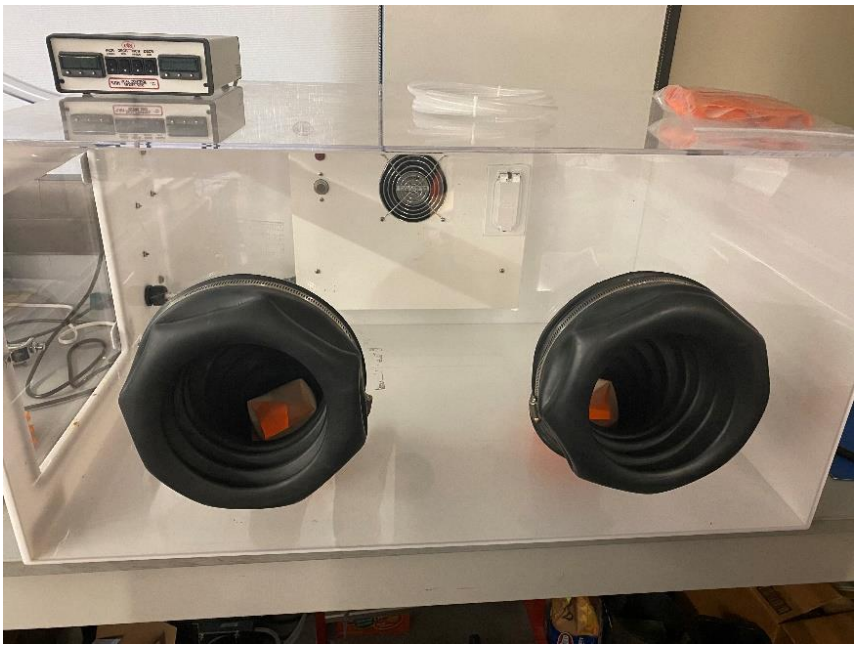

Figure 3.4 Chamber with temperature control panel

According to the manual, the error of the temperature in the chamber is ± 1℃. During the experiment, only the vibrator and sensor would be placed inside while the other component is connected through the wires outside.

The vibrator (V203 LDS) installation is simple. It does not contain any terminal to control its output itself. The vibration generated is decided by a function generator (Model DS345) connecting with it. In this thesis, the vibration is set to the magnitude of 2×10^{-5} with $100\ Hz$ frequency.

A plate clamps the end of the cantilever beam sensor close to the PZT elements with two screws on the basement (Figure 3.5). One more caution is to ensure the plates do not clamp on the PZT element that influences the reaction of the PZT elements.

Figure 3.5 Vibrator with the sensor installed

The amplitude and frequency are known. From equation (2.62), the theoretical value of the charges on the electrodes could be calculated. Equation (3.13) provides the relationship between final output voltage and charge generated on the sensor. Therefore, the theoretical value of the voltage could be plotted in Figure 3.6.

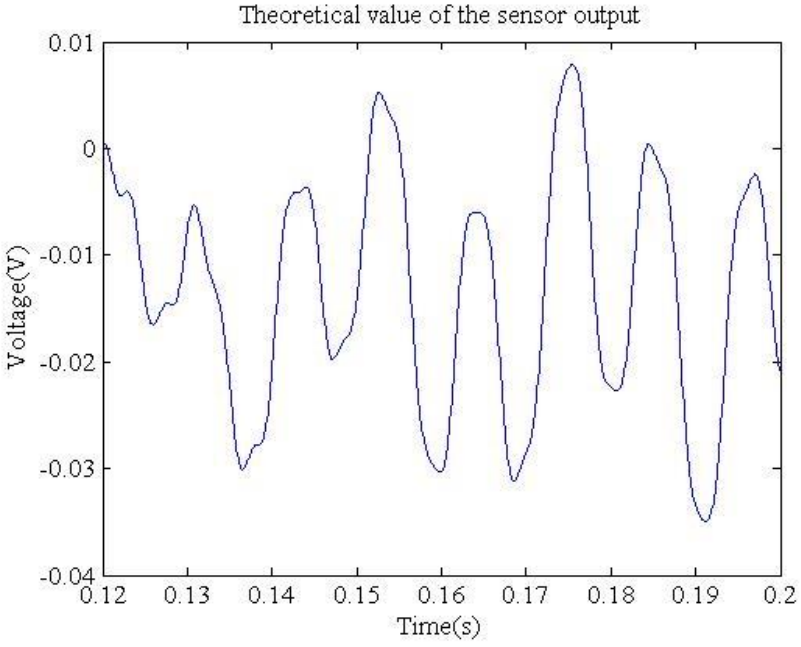

Figure 3.6 Theoretical output of the triple layer sensor

The average peak-to-peak value for the voltage is 29.5 mV. The frequency of the curve is slightly below 100 hz. Since the motion is sinusoid, the acceleration could be represented by $a = U_0\omega^2 \sin(\omega t)$. When the value comes to its maximum, $\sin(\omega t)$ is equal to one. Then, the theoretical sensitivity could be calculated as:

$$S_{v\_theoretical} = \frac{V_{max}}{U_0\omega^2} = \frac{29.5/2\ mV}{2 \times 10^{-8} \times (100 \times 2\pi)^2\ m/s^2} = 1.86\ mV/(m/s^2)\ (3.16)$$

The following step is to calibrate the sensor with a standard accelerometer since the actual output for the experiment is voltage, so practical sensitivity must be calculated based on a known acceleration. The accelerometer is placed on the other plastic basement during the accelerometer calibration. The model of the accelerometer is PCB 352C22 which the sensitivity is 1.0 $mV/(m/s^2)$ [22].

After preparation, the experiment could be started. The flow chart could represent all procedures in Figure 3.7.

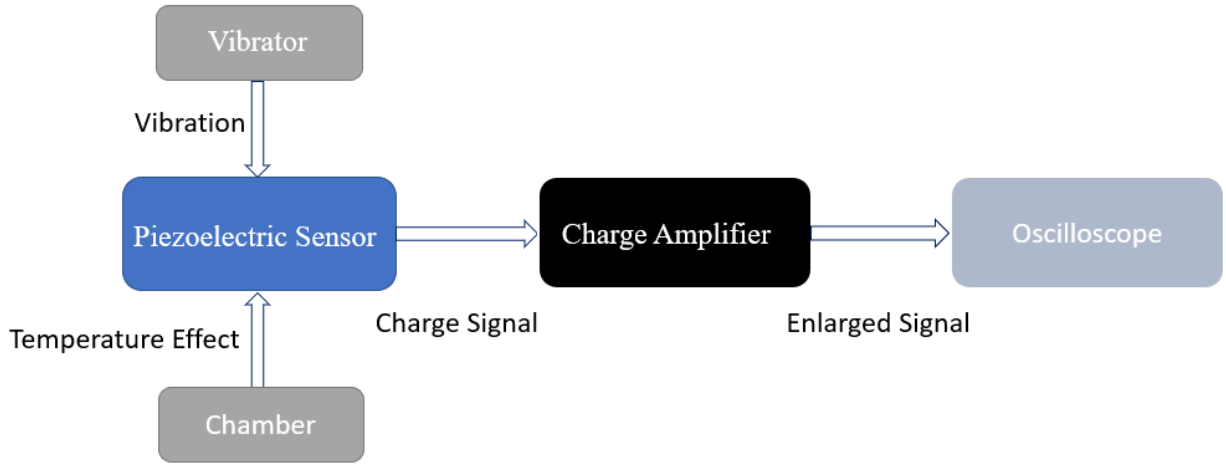

Figure 3.7 The flow chart for the experiment procedure

The actual setup for the experiment is shown in Figure 3.7.

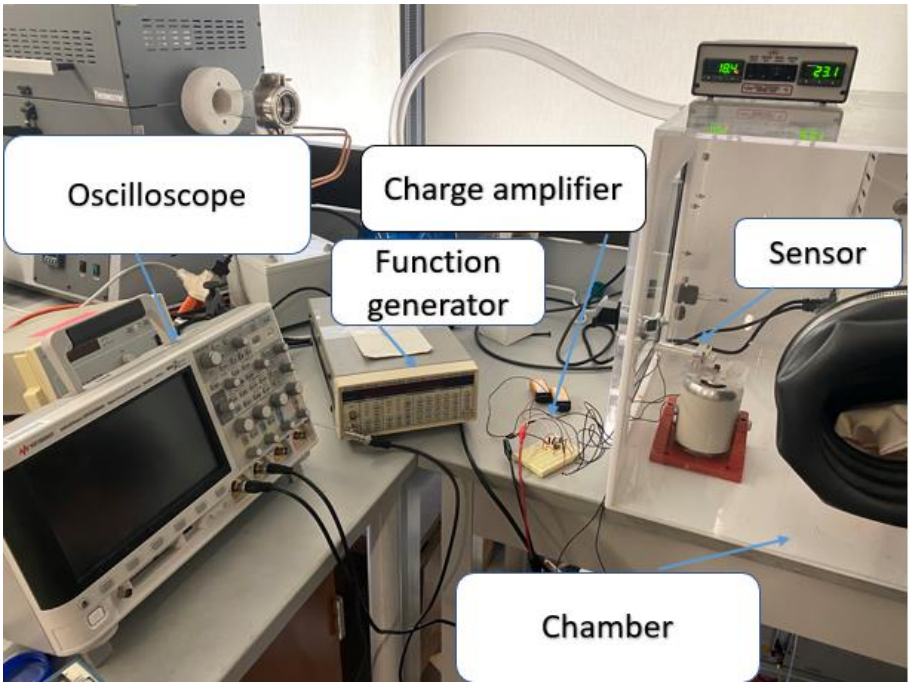

Figure 3.8 Experiment equipment setup

The vibration starts once the temperature reaches the target value during the temperature variation, so the temperature effect exists when the sensor is generating output. After the signal on the oscilloscope is recorded, the temperature is changed to the next desired value. The control panel on the top of the chamber. Once data under four different temperatures is recorded, a unimorph structure sensor should be placed in the chamber and complete the same procedure as trple layer sensor. The unimorph sensor could not cancel the thermal effect by itself, so the result is a good comparison with the triple layer sensor's output.

4.0 Results and Discussion

The result begins with analyzing the calibration data of the triple layer sensor. List the output of the PCB 352C22 sensor and the triple layer sensor in the same figure (Figure 4.1), and it could be seen that the crest and trough of the two curves match with each other. However, the output of the bimorph sensor contains noises that make it hard to distinguish the peak value of the data.

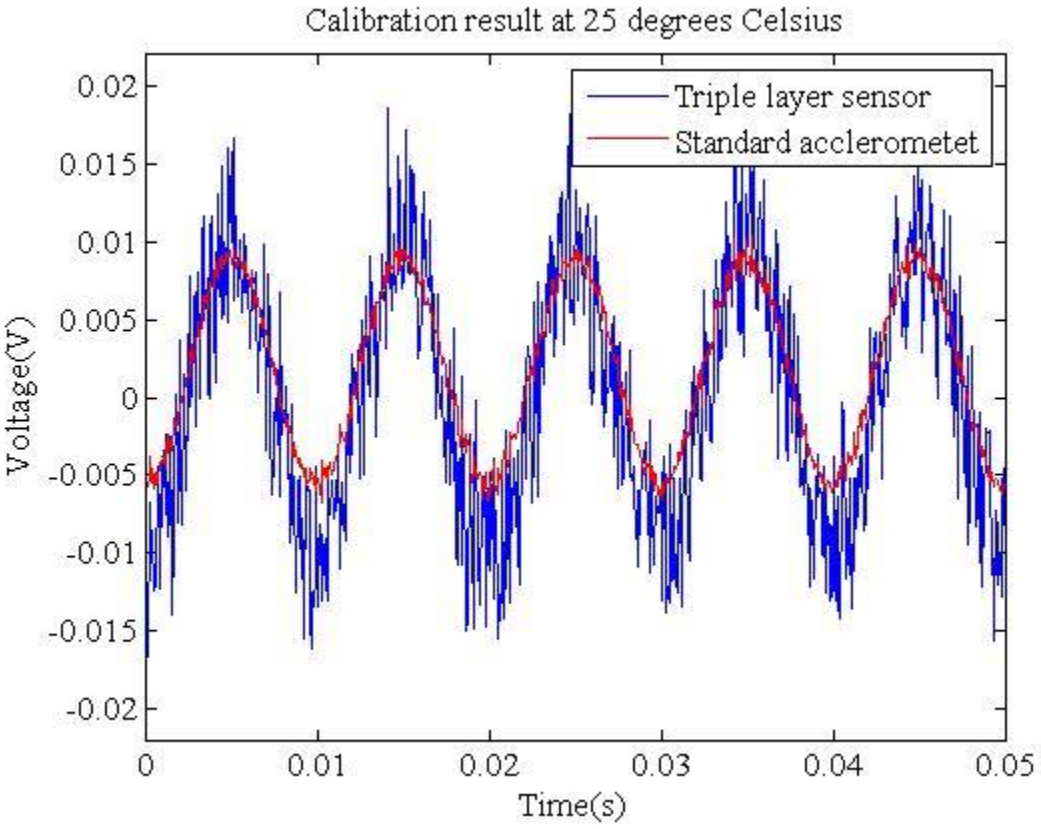

Figure 4.1 The calibration result at 25℃

Therefore, the Fast Fourier transform and the Inverse Fast Fourier transform with filtering process are applied to get a smooth result. After the filtering, the result (Figure 4.2)

becomes readable. The peak-to-peak value for both curves could be found as 16.2 mV for the standard sensor and 26.5 mV for the triple layer sensor. Comparing the practical result with the theoretical value 29.5 mV, the difference is 11% which at a reasonable level. The error might be caused by the following reasons: the loss in wire transportation, the sensor could not be an ideal triple layer structure, or error in variables between the value for calculation and the actual value.

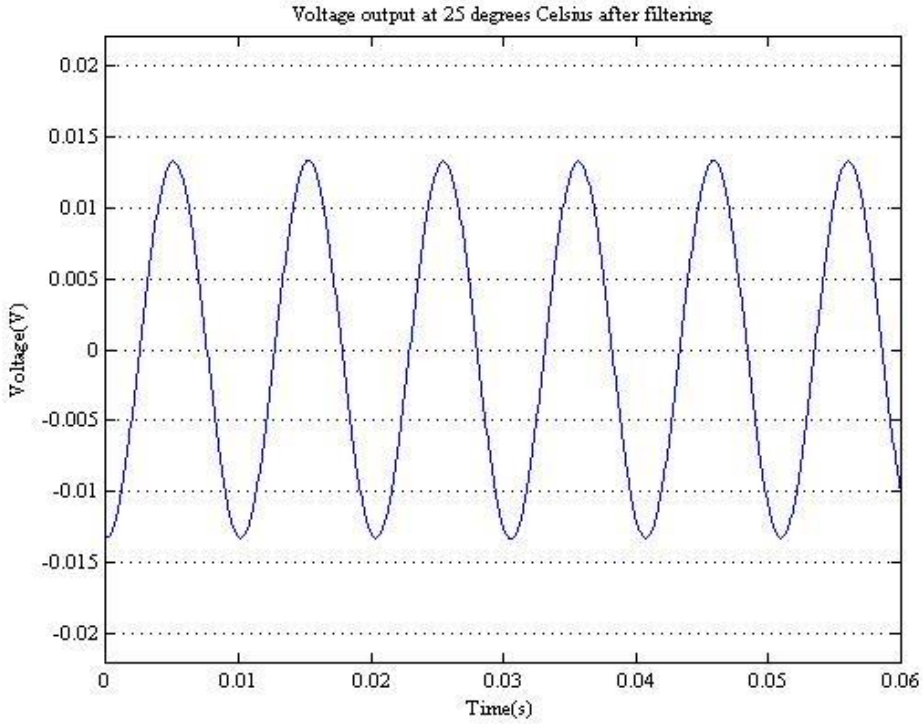

Figure 4.2 The bimorph sensor voltage output after filtering

According to the previous section, the sensitivity of the standard sensor is $1mv/(m/s^2)$. Consequently, the sensitivity of the bimorph sensor could be calculated:

$$S_{v\_practical} = \frac{26.5\,mV}{16.2\,mV\ \times 1\ mv/(m/s^2)} = 1.636\,mv/(m/s^2) \qquad (4.1)$$

According to the value in equation (3.16), the difference in the sensitivity between the theoretical and practical value is 12 %.

To indicate the temperature stability, totally four groups of results at different temperatures are recorded for the triple layer sensor and the unimorph structure sensor. The original and processed results of the triple layer are shown in Figure 4.3 and Figure 4.4.

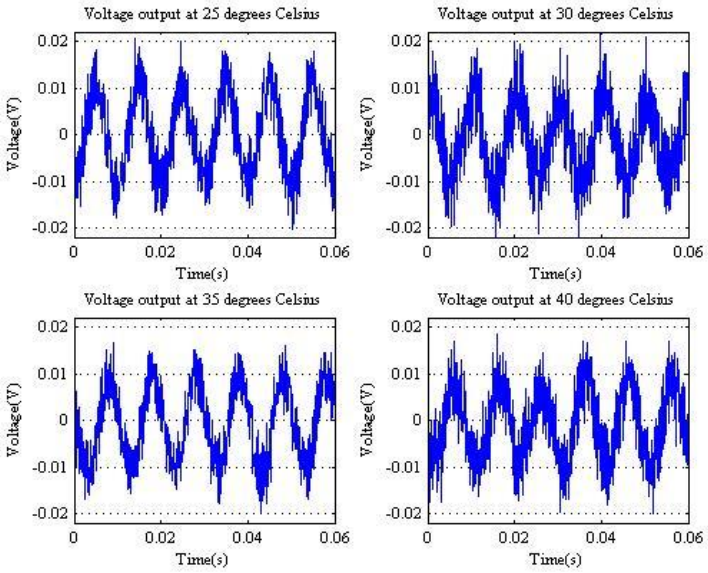

Figure 4.3 The original voltage output

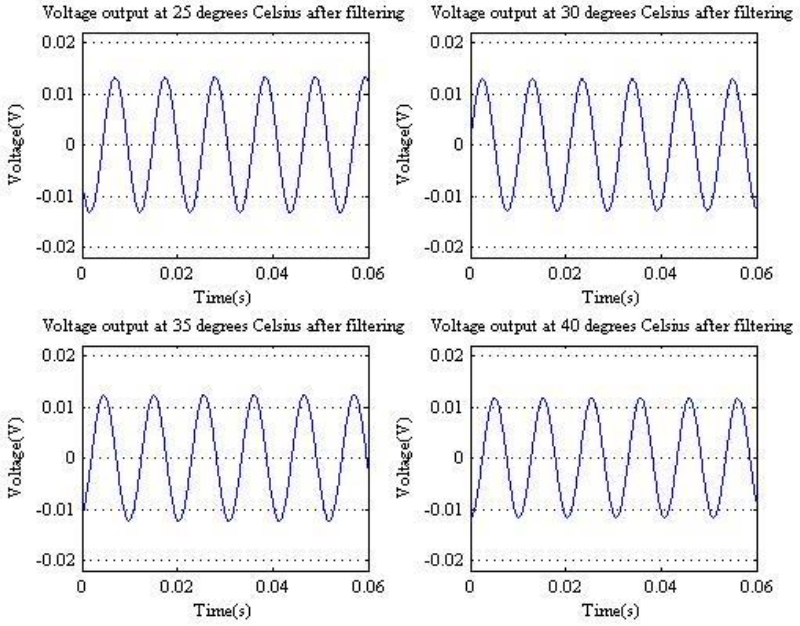

Figure 4.4 The processed voltage output

To have a clearer view, the output is put in the same plot in Figure 4.5.

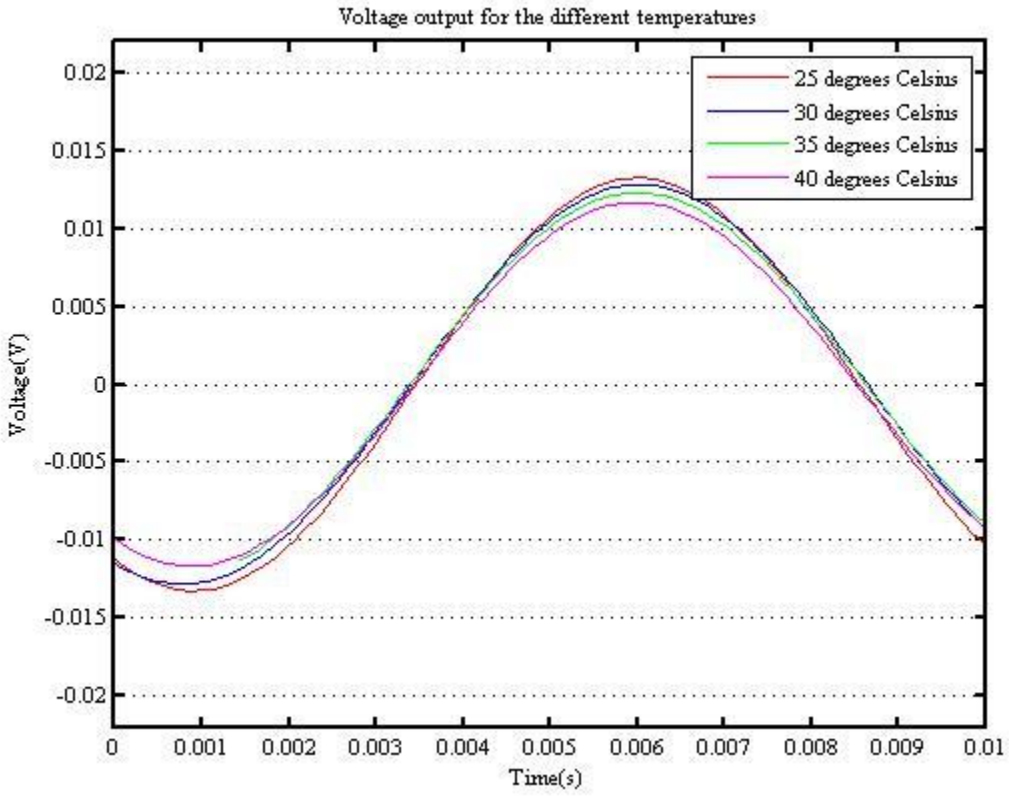

Figure 4.5 Output voltage under different temperatures

The shape of the curve remains the same, as well as the peak value changes slightly. The peak-to-peak value under different temperatures is shown in Table 4-1, and the sensitivity deviation in percentage with respect to temperature is plotted in Figure 4.6.

Table 4-1 The peak-to-peak value of the voltage and sensitivity deviation at different temperature

Temperature (℃)	Peak-to-peak value (mV)	Sensitivity deviation (%)
25	26.5	0
30	26.1	-1.51
35	25.4	-4.15
40	24.6	-7.17

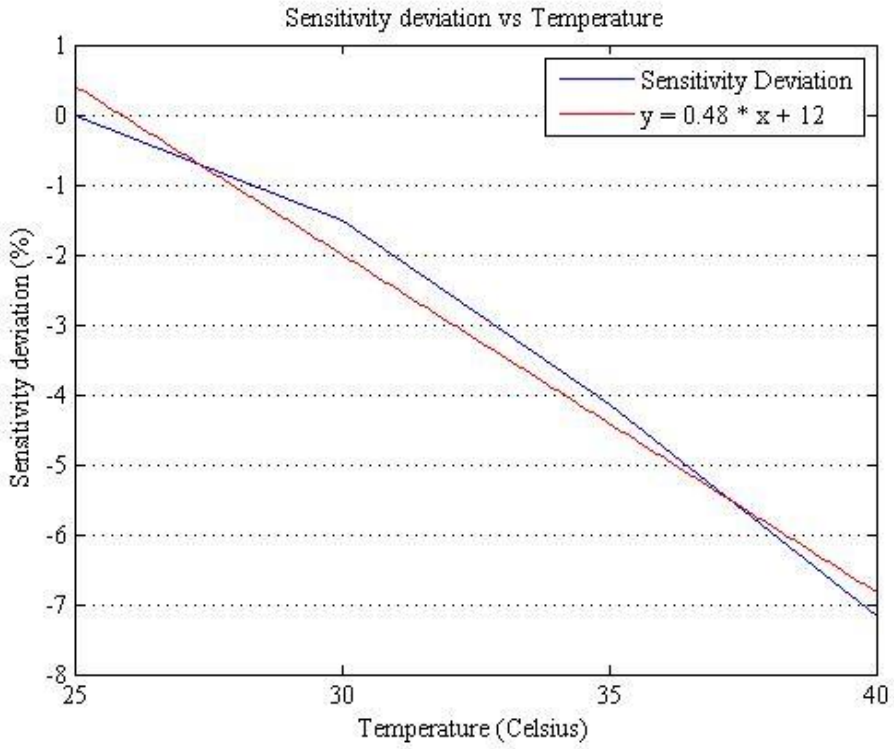

Figure 4.6 Sensitivity deviation along with the temperature change

The result is not perfectly linear but with the trend to have more deviation at high temperature. The total deviation from 25 ℃ to 40 ℃ is 7.17 % for the triple layer sensor. Compared to the sensitivity deviation of the PCB 355C2 sensor (Figure 4.7) at the same range, which is about 2.5 %, it is an acceptable value.

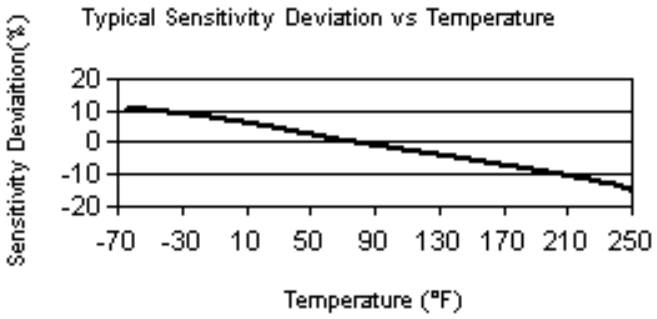

Figure 4.7 Sensitivity deviation of PCB 355C2 under different temperatures [22]

The unimorph sensor output is shown below in Figure 4.8.

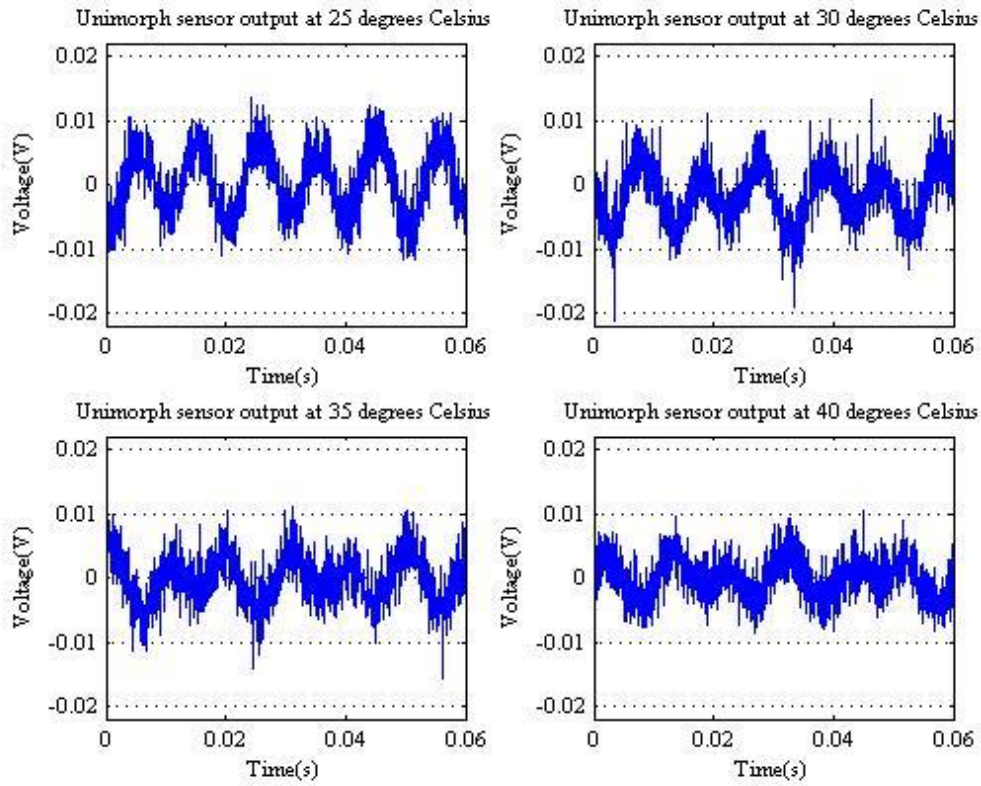

Figure 4.8 Unimorph sensor output at different temperature

It could be seen that the initial output at 25 ℃ is stable and have a peak value around 7.5 $m\,V$. When the temperature elevates to 30℃, the signal is no longer stable and generate irregular output. At the same time, the maximum value decreases. As the temperature continues rising, the signals become more unstable, and the shape shrinks, which means it could not work functionally under high temperature because of temperature instability.

5.0 Conclusion

The objective of the experiment is to indicate the sensor's thermal stability under elevated temperature by designed it with an appropriate structure.

Even with the pyroelectric effect, the PZT materials are still preferred since they make up most of the disadvantages of the traditional mass loaded physical sensor, as well as it is one of the cheapest materials among the piezoceramic. After reviewing the structure of the flexural piezoelectric sensor, the triple layer sensor in parallel connection is selected to test. The structure owns the temperature compensation function and theoretically stable signal under elevated temperature. The static and dynamic response is analyzed to discuss the factors that determine the output of the sensor.

In the experiment, both the triple layer and the unimorph sensor are tested under the same condition. The output for triple layer sensor is stable as temperature increases, while the unimorph sensor only generates an unreliable output that does not reflect the motion of the beam.

There are several aspects of the experiment that could be improved. The first one is about the noise of the output. Although a charge amplifier is applied, the output is still relatively small. The noise makes output curve distortion. The fast Fourier transform could filter the noise out. Meanwhile, the processed signal loses its accuracy compared with the original put. A vibrator that can generate a more considerable amplitude vibration might change the situation.

Another thing is about the deviation of the theoretical value. The results might not be reliable since the frequency does not fit the actual situation and the curve is irregular. The numerical method such as finite element analysis should choose when the numerical solution is not available.

Bibliography

[1] D. A. Van Den Ende, W. A. Groen, and S. Van Der Zwaag, "Development of temperature stable charge based piezoelectric composite quasi-static pressure sensors," *Sensors Actuators, A Phys.*, vol. 163, no. 1, pp. 25–31, 2010, doi: 10.1016/j.sna.2010.06.010.

[2] K. Govind, A. Pahwa, N. Aggarwal, and V. Balodhi, "Ecosecurity energy harvesting using piezoelectric crystal," *2012 Students Conf. Eng. Syst. SCES 2012*, 2012, doi: 10.1109/SCES.2012.6199116.

[3] "Piezoelectricity - Wikipedia." https://en.wikipedia.org/wiki/Piezoelectricity (accessed Mar. 29, 2021).

[4] Maiti and Bidinger, *Piezoelectricity*, vol. 53, no. 9. 1981.

[5] K. R. Rashmi, A. Jayarama, N. Navin Bappalige, and R. Pinto, "A Review on Vibration Based Piezoelectric Energy Harvesters," *Sahyadri Int. J. Res.*, vol. 3, no. 1, pp. 47–56, 2017.

[6] P. Duran and C. Moure, "Piezoelectric ceramics," *Materials Chemistry and Physics*, vol. 15, no. 3–4. pp. 193–211, 1986, doi: 10.1016/0254-0584(86)90001-5.

[7] T. L. Jordan and N. Langley, "Piezoelectric Ceramics Characterization," 2001.

[8] S. J. Rupitsch, "Piezoelectric Sensors and Actuators," *Simulation of Piezoelectric Sensor and Actuator Devices. In: Piezoelectric Sensors and Actuators. Topics in Mining, Metallurgy and Materials Engineering*. pp. 83–126, 2019, [Online]. Available: http://link.springer.com/10.1007/978-3-662-57534-5.

[9] R. Müller-Fiedler and V. Knoblauch, "Reliability aspects of microsensors and micromechatronic actuators for automotive applications," *Microelectron. Reliab.*, vol. 43, pp. 1085–1097, 2003.

[10] H. Fukada Tetsuji, Masayuki Wakamiya, both of Suita;Kikuo Kainou, "Vibration/Acceleration Sensor," US5003824, 1991.

[11] S. Zhang, X. Jiang, M. Lapsley, P. Moses, and T. R. Shrout, "Piezoelectric accelerometers for ultrahigh temperature application," *Appl. Phys. Lett.*, vol. 96, no. 1, 2010, doi: 10.1063/1.3290251.

[12] M. Gries, R. Giles, D. Kuchma, B. Spencer, L. Bergman, and J. Wilcoski, "Advanced Bridge Capacity and Structural Integrity Assessment Methodology," Mar. 2013.

[13] W. H. Duan, Q. Wang, and S. T. Quek, "Applications of Piezoelectric Materials in Structural Health Monitoring and Repair: Selected Research Examples.," *Mater. (Basel, Switzerland)*, vol. 3, no. 12, pp. 5169–5194, Dec. 2010, doi: 10.3390/ma3125169.

[14] L. Qin *et al.*, "Fabrication and characterization of thick-film piezoelectric lead zirconate titanate ceramic resonators by tape-casting," *IEEE Trans. Ultrason. Ferroelectr. Freq. Control*, vol. 59, no. 12, pp. 2803–2812, 2012, doi: 10.1109/TUFFC.2012.2522.

[15] M. TODA, *Design of piezoelectric polymer motional devices with various structures*, vol. 61, no. 7. The Institute of Electronics, Information and Communication Engineers, 1978.

[16] J. G. Smits, S. I. Dalke, and T. K. Cooney, "The constituent equations of piezoelectric bimorphs," *Sensors Actuators A Phys.*, vol. 28, no. 1, pp. 41–61, 1991, doi: https://doi.org/10.1016/0924-4247(91)80007-C.

[17] Q. M. Wang and L. Eric Gross, "Constitutive equations of symmetrical triple layer piezoelectric benders," *IEEE Trans. Ultrason. Ferroelectr. Freq. Control*, vol. 46, no. 6, pp. 1343–1351, 1999, doi: 10.1109/58.808857.

[18] P. M. Morse and K. U. Ingard, *Theoretical acoustics*. New York: McGraw-Hill, 1968.

[19] I. Jung and Y. Roh, “Design and fabrication of piezoceramic bimorph vibration sensors,” *Sensors Actuators A Phys.*, vol. 69, no. 3, pp. 259–266, 1998, doi: https://doi.org/10.1016/S0924-4247(98)00099-5.

[20] “Piezoelectric sensor - Wikipedia.” https://en.wikipedia.org/wiki/Piezoelectric_sensor (accessed Mar. 24, 2021).

[21] “Time constant - Wikipedia.” https://en.wikipedia.org/wiki/Time_constant (accessed Mar. 18, 2021).

[22] “PCB Model 352C22.” https://www.pcb.com/products?m=352C22 (accessed Mar. 18, 2021).